

Two staggered circular cylinders of equal diameter in cross-flow

D. Sumner*, M.D. Richards, O.O. Akosile

Department of Mechanical Engineering, University of Saskatchewan, 57 Campus Drive, Saskatoon, Sask., Canada S7N 5A9

Received 12 December 2003; accepted 18 October 2004

Available online 21 January 2005

Abstract

Wind tunnel experiments were conducted to measure the mean aerodynamic forces and vortex shedding frequencies for two staggered circular cylinders of equal diameter in cross-flow. The Reynolds number based on cylinder diameter ranged from $Re = 3.2 \times 10^4$ to 7.4×10^4 , the centre-to-centre pitch ratio was varied from $P/D = 1.125$ to 4.0, and the incidence angle was incremented in small steps from $\alpha = 0^\circ$ to 90° . The mean drag and lift force coefficients and the Strouhal numbers were obtained for both the upstream and downstream cylinders. From the behaviour of the experimental data, the staggered configuration could be broadly classified by the pitch ratio as closely spaced ($P/D < 1.5$), moderately spaced ($1.5 \leq P/D \leq 2.5$), or widely spaced ($P/D > 2.5$). Closely spaced staggered cylinders are characterized by mean aerodynamic forces that undergo large changes in magnitude and direction with the incidence angle for both cylinders. The same Strouhal number is measured behind both cylinders, an indication of single-bluff-body behaviour. Moderately spaced staggered cylinders are characterized by small changes in the mean aerodynamic forces on the upstream cylinder, but a relatively complex behaviour of the mean aerodynamic forces on the downstream cylinder. Two Strouhal numbers are measured for most incidence angles. For both closely spaced and moderately spaced configurations, a critical incidence angle was found that is associated with a local maximum drag coefficient on the upstream cylinder, a maximum inward-directed lift coefficient for the downstream cylinder (known as the inner lift peak), a local minimum drag coefficient for the downstream cylinder, and a maximum value for the Strouhal number. Widely spaced staggered cylinders are characterized by mean aerodynamic forces on the upstream cylinder that are mostly unchanged from the single cylinder, and a single Strouhal number for both cylinders indicative of synchronized vortex shedding from both cylinders at all incidence angles. The mean aerodynamic forces on the downstream cylinder are marked by a minimum drag coefficient in the tandem configuration and the appearance of the outer lift peak. The outer lift peak for the downstream cylinder is associated with the proximity or impingement of shed Kármán vortices from the upstream cylinder.

© 2004 Elsevier Ltd. All rights reserved.

1. Introduction

Because of its common occurrence in many forms and in different applications, fluid flow around a circular cylinder has been well studied and is one of the classical problems of fluid mechanics. Cylinder-like structures can be found both alone and in groups in the designs for heat exchangers, cooling systems for nuclear power plants, offshore structures,

*Corresponding author. Tel.: +1 306 966 5537; fax: +1 306 966 5424.

E-mail address: david.sumner@usask.ca (D. Sumner).

buildings, chimneys, power lines, struts, grids, screens, and cables, in both air- and water flow. In many of these engineering applications, Kármán vortex shedding is responsible for problems with flow-induced vibration and noise. A complete understanding of the fluid dynamics for the flow around a circular cylinder includes such fundamental subjects as the boundary layer, separation, the free shear layer, the wake, and the dynamics of vortices.

Less well studied and understood are the changes to the flow around a single circular cylinder which may occur when two or more circular cylinders are placed in close proximity to one another. The flow fields of multiple-cylinder configurations involve complex interactions between the shear layers, vortices and Kármán vortex streets; see the reviews of Zdravkovich (1977, 1987, 1993, 2003); Nishimura (1986); Chen (1987); and Ohya et al. (1989). The staggered configuration is the most general arrangement of two circular cylinders. The geometry of the staggered pair of cylinders, each of the same diameter, D , immersed in steady cross-flow of velocity U , is set by the centre-to-centre pitch, P , between the cylinders and the angle of incidence, α , Fig. 1(a). Alternatively, the arrangement of the cylinders has been defined by some authors using the longitudinal and transverse spacings, L and T , respectively, Fig. 1(b).

The staggered configuration has been studied primarily from an experimental approach, and mostly at high subcritical Reynolds numbers (defined for a single circular cylinder), since these are more commonly found in industrial applications; otherwise, the effects of Reynolds number on the staggered configuration have not been systematically studied. Because of the complexity of the flow, there have been relatively few numerical studies of the staggered configuration. Mittal et al. (1997) modeled the flow at $Re = 100$ and 1000 for a widely spaced staggered configuration of $P/D = 5.54$ and $\alpha = 7.25^\circ$. Jester and Kallinderis (2003) modelled the staggered cylinders at $Re = 80$ – 1000 and had some success at reproducing the experimentally observed flow patterns.

The previous experimental studies of the staggered configuration have revealed considerable complexity in the fluid dynamics, as the centre-to-centre pitch ratio, P/D , and α are varied (or, alternatively, the longitudinal and transverse pitch ratios, L/D and T/D , respectively); a large number of these studies are summarized in Table 1. The complexity of the flow arises from the interaction of four separated free shear layers, two Kármán vortex formation and shedding processes, and interactions between the two Kármán vortex streets, Fig. 1(c). A number of approaches have been followed in an attempt to classify the fluid behaviour around staggered circular cylinders immersed in steady cross-flow. Zdravkovich (1987) classified the fluid behaviour into two basic types of interference, based on the location of the

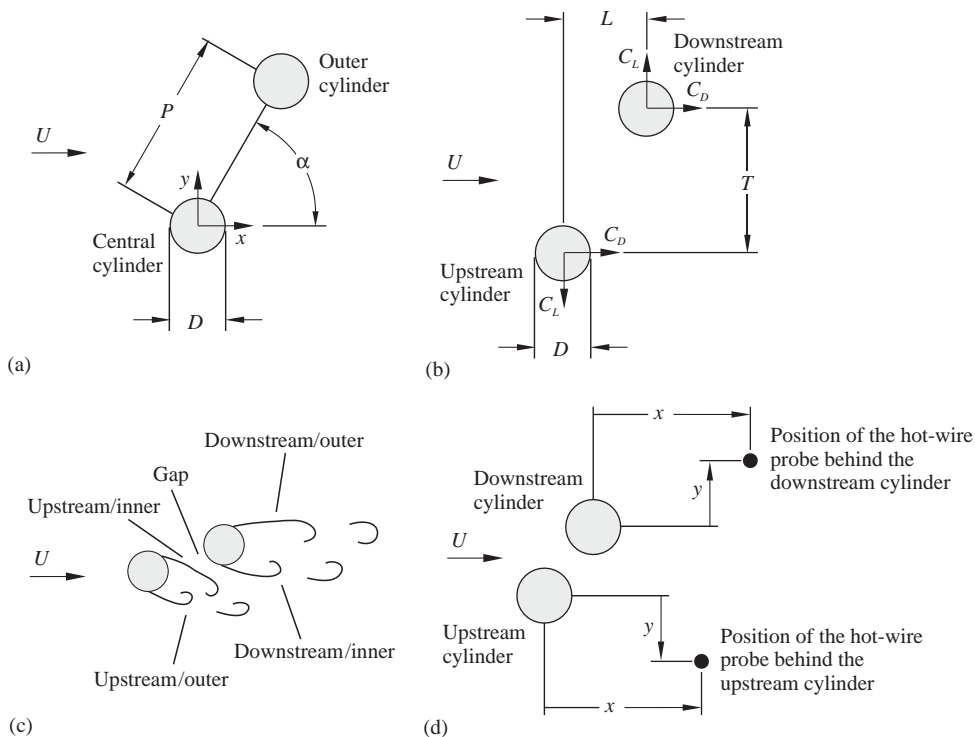


Fig. 1. Staggered configuration of two circular cylinders of equal diameter in steady cross-flow: (a) P/D - α notation; (b) L/D - T/D notation, with force conventions for the two cylinders; (c) shear layer and vortex designations; (d) position of the hot-wire probe relative to the upstream and downstream cylinders.

Table 1
Experimental studies of two staggered circular cylinders of equal diameter in steady cross-flow

Researchers	Re	Geometry	AR	Blockage	TI_u	Method	Measurements
Akosile and Sumner (2003)	5.0×10^4	$P/D = 1.125\text{--}1.25$ $\alpha = 0\text{--}90^\circ$	17.6	3.5%	0.6%	Wind tunnel Force balance, CTA, pressure	C_D, C_L, St C_{PB}
Bokaian and Geoola (1984)	5900	$L/D = 1.5\text{--}4.0$ $T/D = 0.0\text{--}6.0$	18.1	10.7%	6.5%	Water flume Force balance	C_D, C_L
Cooper (1974)	$1.0 \times 10^4\text{--}1.25 \times 10^5$	$L/D = 1.35\text{--}50.51$ $T/D = 0.0\text{--}7.43$	24	8%	Not given	Wind tunnel Force balance, pressure	C_D, C_L C_P
Gu and Sun (1999)	5600	$P/D = 1.5\text{--}2.0$ $\alpha = 0\text{--}45^\circ$	Not given	Not given	Not given	Wind tunnel FV	
Gu and Sun (1999)	$2.2 \times 10^5\text{--}3.3 \times 10^5$	$P/D = 1.1\text{--}3.5$ $\alpha = 0\text{--}90^\circ$	6.4	8%	0.2%	Wind tunnel Pressure	C_D, C_L, St C_P
Gu et al. (1993)	6.5×10^5	$P/D = 1.05\text{--}4.0$ $\alpha = 0\text{--}90^\circ$	15	11.4%	0.12–10.0%	Wind tunnel Pressure	C_D, C_L C_P
Ishigai et al. (1972, 1973)	$1500\text{--}1.5 \times 10^4$	$L/D = 0.68\text{--}4.0$ $T/D = 0.5\text{--}3.0$	11	9%	Not given	Wind tunnel FV, CTA, pressure	St C_P
Kiya et al. (1980)	$2.0 \times 10^4\text{--}3.7 \times 10^4$	$P/D = 0.0\text{--}5.5$ $\alpha = 0\text{--}90^\circ$	11	19%	0.8%	Wind tunnel CTA	St
Moriya and Sakamoto (1985)	6.53×10^4	$L/D = 2.0\text{--}6.0$ $T/D = 0.0\text{--}1.5$	10	20%	0.4%	Wind tunnel Force balance, FV, pressure	C_D, C_L, St
Ozono et al. (2001)	2500–7500	$L/D = 1.0\text{--}4.0$ $T/D = 0.0\text{--}2.0$	23.3	7.5%	1.0%	Water channel FV, CTA	C_P, C_P', C_D', C_L'
Ozono et al. (2001)	3.0×10^4	$L/D = 1.0\text{--}4.0$ $T/D = 0.0\text{--}2.0$	14.6	8.8%	2.0%	Wind tunnel CTA, pressure	St C_{PB}
Price (1976)	$1.7 \times 10^4\text{--}8.0 \times 10^4$	$L/D = 6.0\text{--}18.0$ $T/D = 0.0\text{--}2.42$	37, 42	5–12%	1.0–11.0%	Wind tunnel Force balance, FV, pressure	C_P, C_D, C_L
Price and Paidoussis (1984)	$1.7 \times 10^4\text{--}8.6 \times 10^4$	$L/D = 1.5\text{--}5.0$ $T/D = 0.75\text{--}2.0$	24	6%	0.5%	Wind tunnel Force balance	C_D, C_L
Sun et al. (1992)	$3.25 \times 10^5\text{--}6.5 \times 10^5$	$P/D = 2.2$ $\alpha = 12.5^\circ$	15	10%	0.12–10.0%	Wind tunnel Pressure	C_P, C_P'
Sumner (2004)	5.0×10^4	$P/D = 1.125\text{--}1.25$ $\alpha = 0\text{--}90^\circ$	17.6	3.5%	0.6%	Wind tunnel Force balance, CTA, pressure	C_D, C_L, St C_{PB}
Sumner et al. (2000)	850–1350	$P/D = 1.0\text{--}5.0$ $\alpha = 0\text{--}90^\circ$	16	13%	0.5%	Water tunnel FV	St
Sumner et al. (2000)	1900	$P/D = 1.0\text{--}4.0$ $\alpha = 0\text{--}90^\circ$	27	7%	—	Towing tank PIV	
Sumner and Richards (2003)	$3.2 \times 10^4\text{--}7.0 \times 10^4$	$P/D = 2.0\text{--}2.5$ $\alpha = 0\text{--}90^\circ$	24	5.6%	0.6%	Wind tunnel Force balance, CTA	C_D, C_L, St
Suzuki et al. (1971)	1300	$P/D = 2.0$ $\alpha = 0\text{--}15^\circ$	Not given	Not given	Not given	Water tunnel FV	
Suzuki et al. (1971)	$1.0 \times 10^5\text{--}6.3 \times 10^5$	$P/D = 1.1\text{--}3.9$ $\alpha = 0\text{--}15^\circ$	6–18	12–24%	Not given	Wind tunnel Pressure	C_D C_P
Ting et al. (1998)	$4.0 \times 10^4\text{--}2.0 \times 10^5$	$L/D = 1.5\text{--}5.0$ $T/D = 0.1\text{--}1.05$	5.3–12.8	10.6–25%	0.8%	Wind tunnel Force balance, pressure	C_D, C_L
Wardlaw and Cooper (1973)	$1.2 \times 10^4\text{--}1.4 \times 10^5$	$P/D = 1.2\text{--}35$ $\alpha = 0\text{--}75^\circ$	45	3%	Not given	Wind tunnel Force balance	C_D, C_L
Zdravkovich and Pridden (1977)	6.0×10^4	$L/D = 0.0\text{--}5.0$ $T/D = 0.0\text{--}3.0$	33	5%	0.1%	Wind tunnel Force balance, pressure	C_D, C_L C_P
Current study	$3.2 \times 10^4\text{--}7.4 \times 10^4$	$P/D = 1.125\text{--}4.0$ $\alpha = 0\text{--}90^\circ$	17.6, 24	3.5%, 5.6%	0.6%	Wind tunnel Force balance, CTA	C_D, C_L, St

FV = flow visualization; CTA = constant temperature anemometry; PIV = particle image velocimetry. Blockage ratio based on the maximum total blockage for two cylinders.

downstream cylinder with respect to the upstream one: (i) wake interference, when one of the cylinders is partially or completely submerged in the wake of the other, and (ii) proximity interference, when the two cylinders are located close to one another, but neither is submerged in the wake of the other. Gu and Sun (1999) extended this classification to three different types, namely wake interference, shear layer interference, and neighbourhood interference. However, their study was limited to staggered configurations with small and intermediate pitch ratios (see Table 1) in the high subcritical regime ($Re = 2.2 \times 10^5 - 3.3 \times 10^5$). More extensive flow visualization and PIV experiments by Sumner et al. (2000) were conducted within the low subcritical regime ($Re = 850 - 1900$) and revealed a much wider range of flow patterns for the staggered configuration. Nine distinct patterns were identified which incorporated various aspects of shear layer reattachment, alternate vortex shedding from one or both cylinders, vortex splitting, pairing and enveloping, synchronized vortex shedding, and vortex impingement. Based on their results, it is possible to broadly group the fluid behaviour according to whether the staggered cylinders are closely spaced, moderately spaced, or widely spaced, as shown in Fig. 2.

The majority of the studies listed in Table 1 have focused on measurements of the mean aerodynamic forces. The mean drag force is represented by the dimensionless mean drag force coefficient, $C_D (= 2F_D/\rho U^2 D l)$, where F_D is the mean drag force, ρ is the fluid density, and l is the span of the cylinder). Similarly, the mean lift force is represented by the dimensionless mean lift force coefficient, $C_L (= 2F_L/\rho U^2 D l)$, where F_L is the mean lift force). The forces on the cylinders follow the sign convention shown in Fig. 1(b): a repulsive (outward-directed) lift force is assigned a positive sign; an attractive (inward-directed) lift force is assigned a negative sign; and the drag force is always positive in the direction of the flow velocity. Of particular concern have been specific staggered geometries that give rise to extreme values of C_L and C_D on the downstream cylinder. Some noteworthy features of the aerodynamic force data include (i) an “inner” lift peak at small L/D and T/D , where the cylinders are nearly in-line, for which the inward-directed lift force on the downstream cylinder reaches a maximum and is highly sensitive to changes in P/D and α ; (ii) an “outer” inward-directed lift peak, at larger L/D and T/D , that is less sensitive to changes in the geometry; and (iii) a minimum drag region, that coincides with the “inner” lift peak (Zdravkovich and Pridden, 1977). A number of different explanations for the origin of the inner and outer lift peaks have been provided in the literature, which were summarized by Ting et al. (1998).

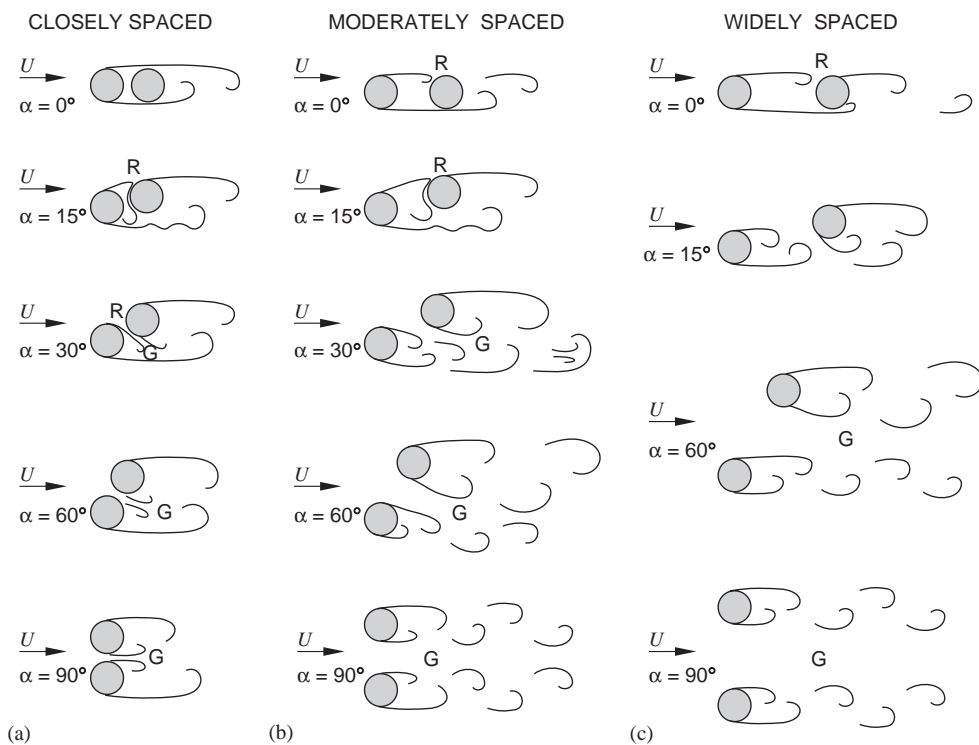


Fig. 2. Overview of flow patterns for two staggered circular cylinders of equal diameter in steady cross-flow, based on Sumner et al. (2000): (a) closely spaced; (b) moderately spaced; (c) widely spaced. R = reattachment; G = gap.

Of the studies from Table 1 that have examined the behaviour of the mean aerodynamic forces, most of them have considered only the downstream cylinder, and have considered only a limited number of staggered configurations, i.e. a limited number of unique combinations of P/D and α (or L/D and T/D). The few studies that have examined the upstream cylinder (Wardlaw and Cooper, 1973; Gu and Sun, 1999; Akosile and Sumner, 2003) have shown that it too may experience large changes in C_L and C_D , particularly at small pitch ratios and incidence angles. An improved understanding is therefore needed of the forces experienced by the upstream cylinder. Because of the limited number of staggered configurations that have been tested, the sensitivity of the mean aerodynamic force coefficients to very small changes in incidence angle is not yet well understood. The sudden appearance and disappearance of the inner lift peak, for example, has not been extensively studied, but could have significant implications in practical applications. Also, the fact that the minimum drag coefficient on the downstream cylinder does not occur when the cylinders are in tandem (Zdravkovich and Pridden, 1977) is another area that needs further study. Additional aerodynamic force coefficient data are therefore needed to answer these and other questions, including clarifying some aspects of the physical relationship between the observed flow patterns and the force coefficient data.

Previous experimental studies of the staggered configuration have focused to a much lesser degree on the vortex shedding frequencies, see Table 1. The vortex shedding frequency, f , is represented in dimensionless form as the Strouhal number, $St (= fD/U)$. For many staggered configurations, two Strouhal numbers are measured (Kiya et al., 1980; Sumner et al., 2000). In other cases, an absence of reliable Strouhal number has been reported for specific combinations of P/D and α , indicating a weakened or absent vortex shedding activity (Sumner and Richards, 2003). However, because of the limited experimental data from previous studies, and the limited number of unique P/D and α combinations tested, the behaviour of the Strouhal number and its sensitivity to the incidence angle still are both not well understood. For example, the inner and outer lift peaks may have counterparts in the Strouhal number data. There too may be other staggered geometries with unreliable Strouhal numbers. There is also evidence from the study of the flow patterns by Sumner et al. (2000) that the Strouhal numbers may be more appropriately associated with individual shear layers rather than the individual cylinders. Additional Strouhal number data, therefore, would be helpful in understanding the physical relationship between the data and the flow field. The behaviour and appearance of the power spectra [addressed only briefly by Kiya et al. (1980)] would be an important consideration also.

In the present study, the mean force coefficients and Strouhal numbers were obtained for both the upstream and downstream cylinders for a wide range of staggered-cylinder configurations. The experiments were undertaken in the subcritical Reynolds number regime, from $Re = 3.2 \times 10^4$ to 7.4×10^4 ; the effects of Reynolds number were not considered, and this subject was left for a future study. Extensive wind tunnel experiments were conducted of staggered configurations with $P/D = 1.125$ – 4.0 and $\alpha = 0$ – 90° . The sensitivity of C_L , C_D , St , and the power spectra were examined by using very small increments in incidence angle, and therefore a large number of staggered arrangements were tested at a given P/D . Few of the previous studies have provided comparable measurements of both the forces and the vortex shedding frequencies in a single set of experiments (see Table 1), hence, it has been difficult to establish the interrelationship between these measurements.

2. Experimental approach

The experiments were conducted in a low-speed, closed-return wind tunnel, with a test-section of 0.91 m (height) \times 1.13 m (width) \times 1.96 m (length). A ground plane was installed near the test-section floor. The experimental set-up is shown in Fig. 3 and is similar to that adopted by Akosile and Sumner (2003) and Sumner and Richards (2003). Under uniform flow conditions, the longitudinal freestream turbulence intensity was less than 0.6% and the velocity non-uniformity in the central portion of the test section, outside the test-section wall boundary layers, was 0.5%.

Two circular cylinders of equal diameter, $D = 0.032$ m, were arranged in staggered configurations corresponding to various combinations of eight pitch ratios, $P/D = 1.125, 1.25, 1.5, 1.75, 2.0, 2.5, 3.0$ and 4.0 , and angles of incidence from $\alpha = 0^\circ$ to 90° . An incidence increment of $1^\circ, 5^\circ$, or 10° was used, depending on the region of interest, which was a smaller increment than in previous studies; a similar approach was adopted by Akosile and Sumner (2003) and Sumner and Richards (2003). The cylinders were tested in the subcritical Reynolds number regime, from $Re = 3.2 \times 10^4$ to 7.4×10^4 . The first cylinder, referred to as the central cylinder in Fig. 3(a), was mounted vertically from a six-component force balance located outside and below the wind tunnel test-section. This cylinder was centrally located in the test-section. The second cylinder was mounted between a pair of circular end plates, referred to as the outer cylinder in Fig. 3(a); details of the end plate design are shown in Fig. 3(b). The end plate design was similar to that adopted by Sumner et al. (2000), and was based on the recommendations of Szepessy (1993) for a single cylinder, with an overall diameter of $P + 7D$. The end plates were positioned away from the test section roof and ground plane on cylindrical supports, as shown in Fig. 3(a), so that the cylinders were located outside the boundary layers developing on these surfaces.

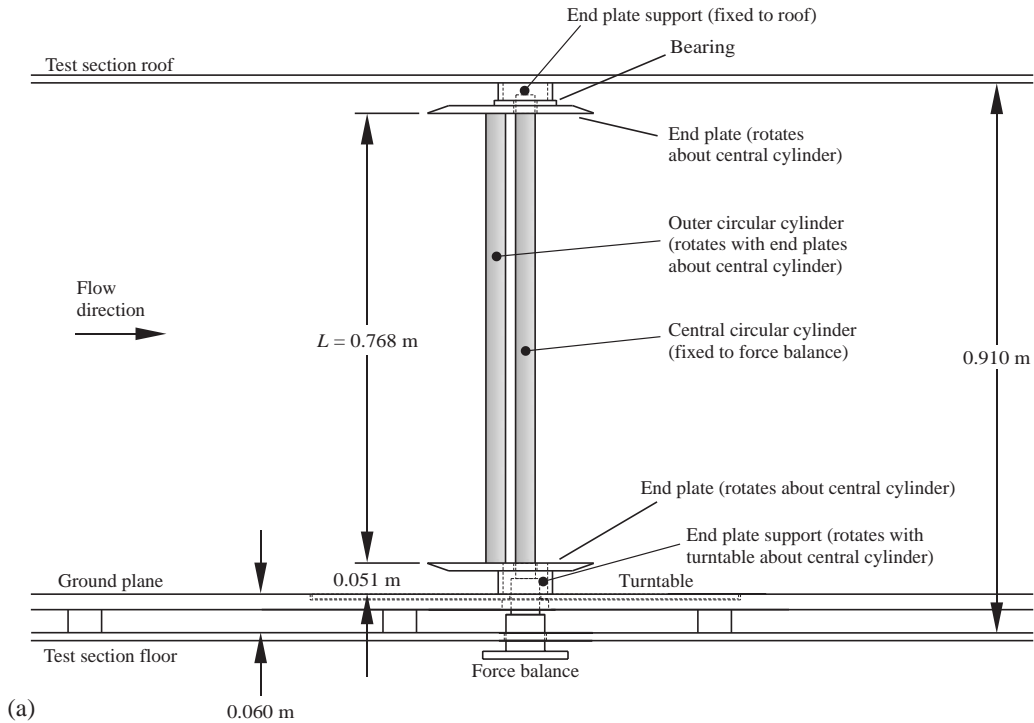


Fig. 3. (a) Experiment set-up in the wind tunnel, $P/D = 1.5$, $\alpha = 0^\circ$; (b) detail of end plates and end plate supports.

The outer cylinder, end plates, and end-plate supports could be rotated in α about the central cylinder using a computer-controlled turntable embedded in the ground plane; see Fig. 3(b). In this way, the central cylinder could represent either an upstream or downstream cylinder over the full range of incidence angle, $\alpha = 0\text{--}90^\circ$. The uncertainty in angular position was estimated at $\pm 0.25^\circ$. The central cylinder was isolated from the outer cylinder and its end plates by a 1 mm gap, as shown in Fig. 3(b). The cylindrical end plate supports surrounded the central cylinder and shielded it from the oncoming flow, see Fig. 3(b), meaning the length of each cylinder that was exposed to the flow was the same. For the majority of the experiments, the cylinder length was $l = 0.768$ m, giving an aspect ratio of $AR = l/D = 24$ and a solid blockage ratio of 2.8% per cylinder; see Fig. 3(a). For the experiments with $P/D = 1.125$ and 1.25, at $Re = 5.0 \times 10^4$ only, the cylinder length was $l = 0.563$ m, giving $AR = 17.6$ and a solid blockage ratio of 1.75% per cylinder. Data from these configurations were reported in an earlier study by Akosile and Sumner (2003), where the installation of a honeycomb shear-flow generator in the test-section reduced the vertical extent of the freestream, and required shorter cylinders to be used (note that the data shown in the present study are for the case of no shear). In all cases, no wall interference corrections were made.

Reference flow conditions were measured with a Pitot-static probe (United Sensor 3.2 mm diameter) and Datametrics Barocell absolute and differential pressure transducers. These data and the force balance data were acquired with a Pentium II microcomputer, a National Instruments AT-MIO-64F-5 12-bit multifunction board and LabVIEW software. Vortex shedding frequencies were measured with a TSI 1210-T1.5 single-component hot-wire probe, a TSI IFA-100 anemometer, a National Instruments PCI-6024E 12-bit data acquisition board, and the National Instruments Virtual Bench Digital Signal Analyzer. The probe was located at mid-span and downstream of the cylinder of interest using a three-axis computer-controlled traversing system. Since the detection of a Strouhal number for the upstream cylinder is highly sensitive to the measurement location (Kiya et al., 1980; Sumner and Richards, 2003), the hot-wire probe was located at various positions to ensure the reliability and repeatability of the power spectra (particularly in the cases where no Strouhal number could be found). The probe was typically positioned at $x/D = 3.0$ and $y/D = 1.0$ from the downstream cylinder, and at $x/D = 3.0$ and $y/D = 1.0$ from the upstream cylinder, see Fig. 1(d). Using the computer-controlled traversing system, the hot-wire probe was repositioned at the same time the outer cylinder was rotated, in order to maintain the same measurement position relative to the cylinders. The measurement uncertainty of the mean lift and drag coefficients was estimated at $C_L \pm 0.02$ and $C_D \pm 0.02$. The measurement uncertainty of the Strouhal number was estimated at $St \pm 0.007$.

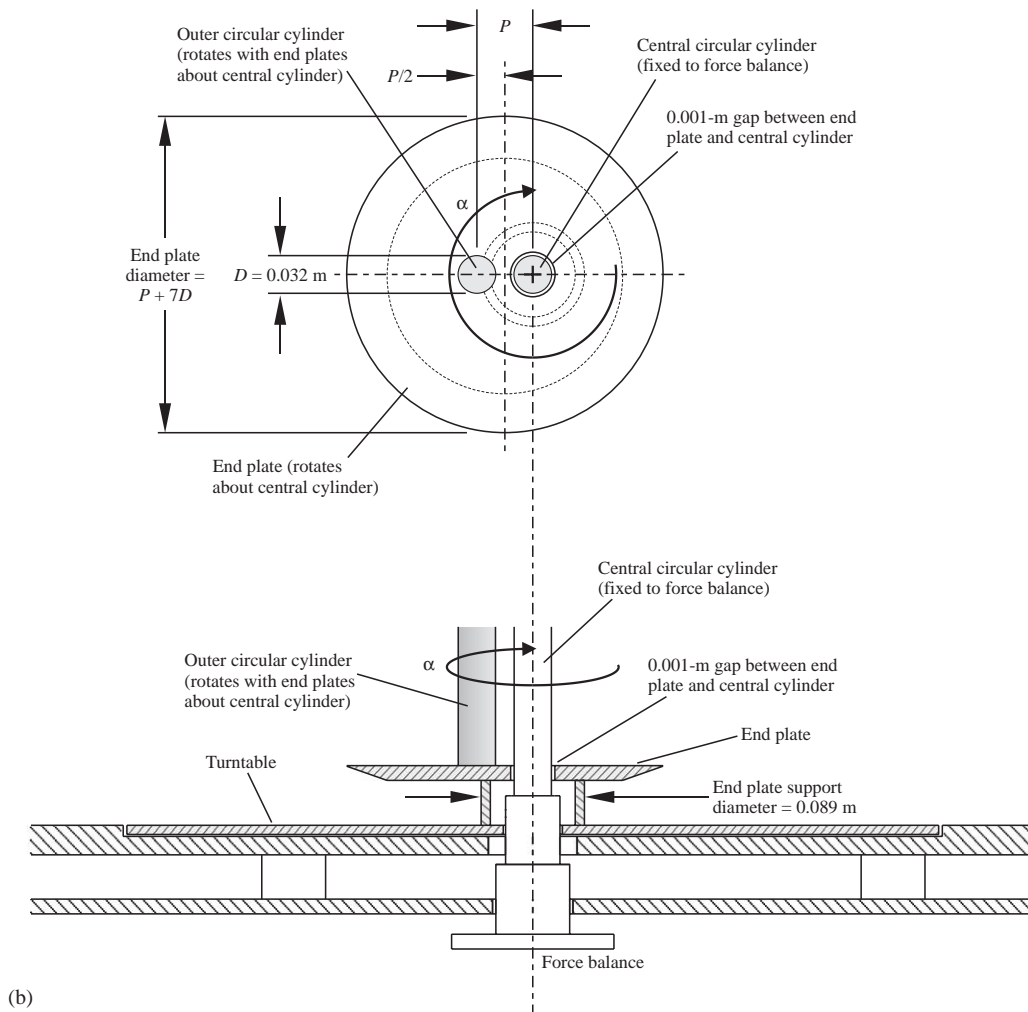


Fig. 3. (Continued)

3. Overview of results

The experimental results for the mean aerodynamic force coefficients, Strouhal numbers, and power spectra, presented in Figs. 4–9, were found to be independent of the Reynolds number within the range that was studied, $Re = 3.2 \times 10^4$ – 7.4×10^4 . The flow pattern boundaries of Gu and Sun (1999), corresponding to the high subcritical Reynolds number regime ($Re = 2.2 \times 10^5$), and Sumner et al. (2000), corresponding to the low subcritical Reynolds number regime ($Re = 850$ – 1900), are included with several of the figures to aid in the interpretation of the data. The force coefficient and Strouhal number data from the present study were consistent with other published data where these data were available. However, to avoid complicating the figures with too much information, previously published data have not been shown in Figs. 4–9. The results in these figures can be used to broadly classify the behaviour of the staggered cylinders using the pitch ratio, into closely spaced ($P/D = 1.125, 1.25$), moderately spaced ($P/D = 1.5, 1.75, 2.0, 2.5$), and widely spaced staggered configurations ($P/D = 3.0, 4.0$), which are described in Sections 4, 5 and 6, respectively.

4. Closely spaced staggered configurations

Closely spaced staggered cylinder configurations of $P/D = 1.125$ and 1.25 behave similar to a single bluff body for nearly the entire range of α , since the cylinders are situated very close to one another and the gap between them is small

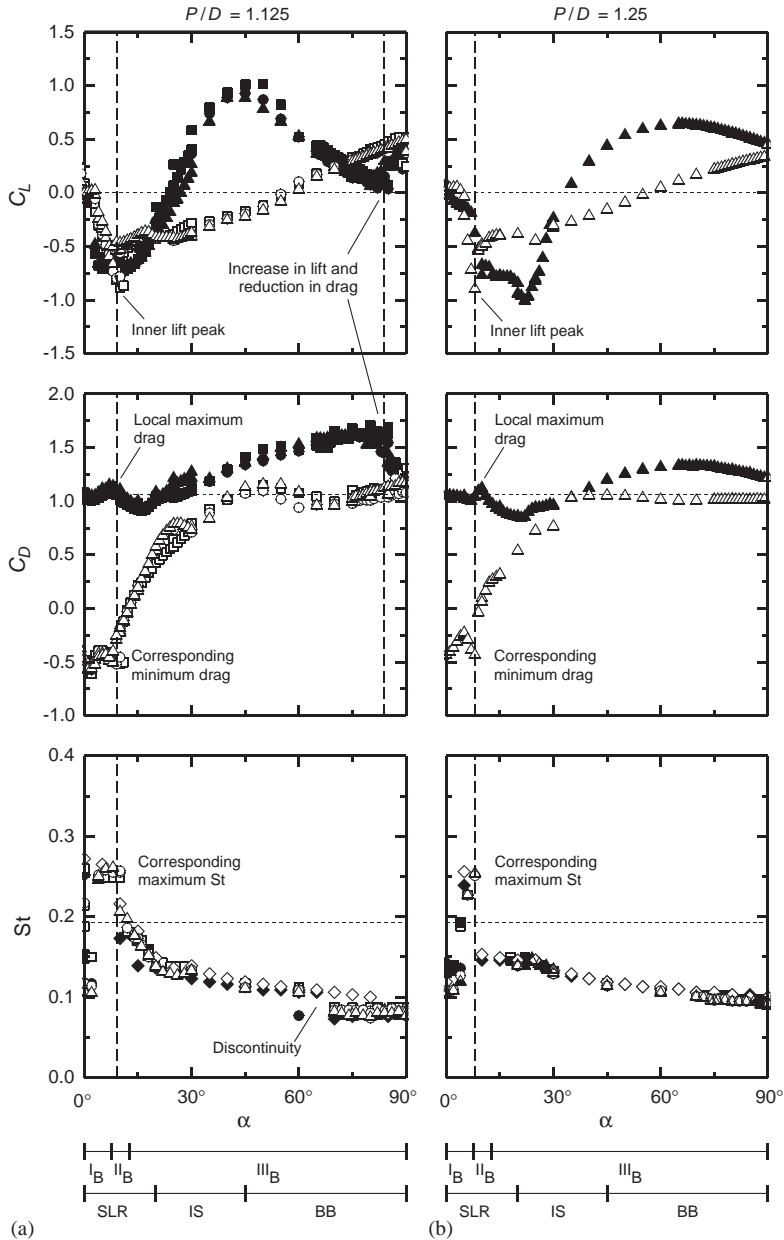


Fig. 4. Closely spaced configurations of two staggered circular cylinders in cross-flow: (a) $P/D = 1.125$; (b) $P/D = 1.25$. ■ or □, $Re = 3.2 \times 10^4$; ◆ or ◇, $Re = 5.0 \times 10^4$; ● or ○, $Re = 5.6 \times 10^4$; ▲ or △, $Re = 7.2 \times 10^4$. Solid symbols: upstream cylinder. Open symbols: downstream cylinder. — — —, Single cylinder. Flow pattern boundaries of Gu and Sun (1999) for $Re = 2.2 \times 10^5$: patterns I_B , II_B , and III_B . Flow pattern boundaries of Sumner et al. (2000) for $Re = 850$ – 1900 : SLR (shear layer reattachment), IS (induced separation), BB (base-bleed).

(Sumner et al., 2000). At these small pitch ratios, Kármán vortex shedding occurs from the cylinder group as a whole rather than from the individual cylinders, and there is single Kármán vortex street in the combined wake (Fig. 2(a)). In the tandem configuration, $\alpha = 0^\circ$, the shear layers from the upstream cylinder wrap around and enclose the downstream cylinder. At small non-zero incidence angles, the inner shear layer from the upstream cylinder either wraps around, or reattaches onto, the downstream cylinder; these are features of the I_B flow pattern of Gu and Sun (1999) and the shear layer reattachment (SLR) flow pattern of Sumner et al. (2000). At larger incidence angles, shear layer reattachment onto

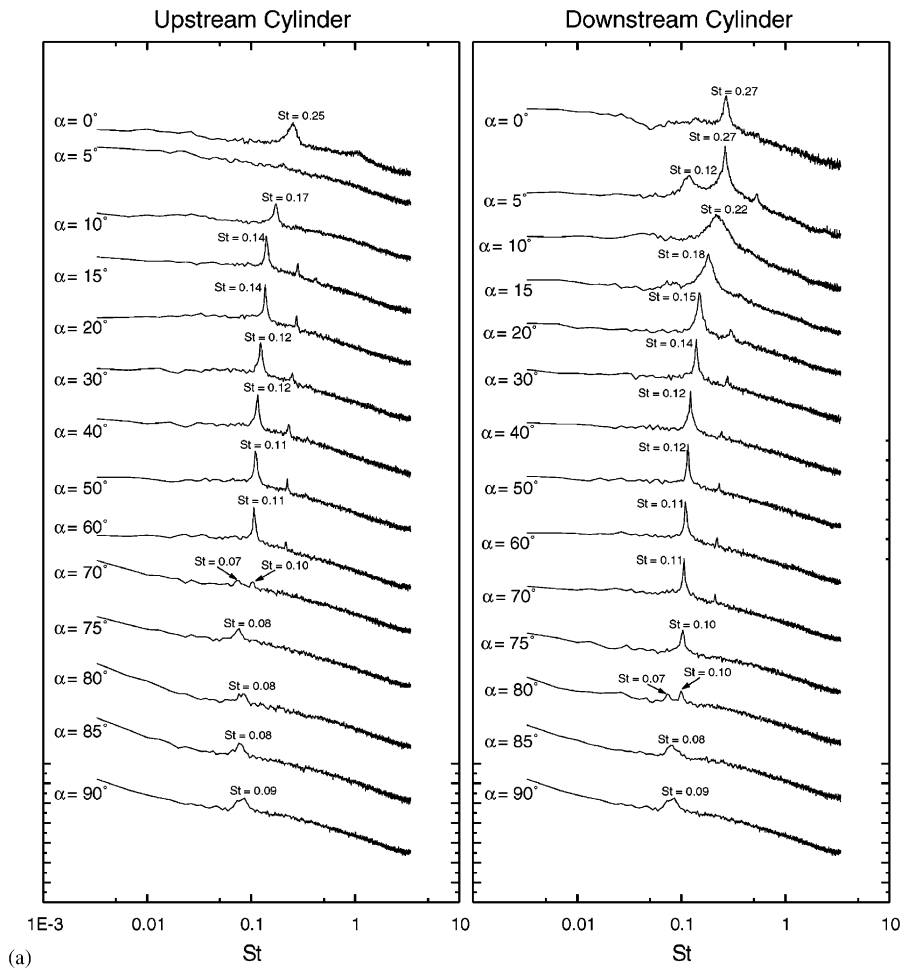


Fig. 5. Selected power spectra, as a function of incidence angle, for closely spaced staggered cylinders: (a) $P/D = 1.125$, $Re = 5.0 \times 10^4$; (b) $P/D = 1.25$, $Re = 5.0 \times 10^4$. Each spectrum represents 250 averages. The vertical (logarithmic) scale is arbitrary, but the same scale is used for each spectrum.

the downstream cylinder can no longer be maintained. Instead, some of the approach flow is directed through the gap between the cylinders and enters the near-wake region. At lower incidence angles, this flow occurs adjacent to the inner side of the downstream cylinder; this is a feature of the II_B flow pattern of Gu and Sun (1999) and the induced separation (IS) flow pattern of Sumner et al. (2000). At larger incidence angles, the gap flow becomes more significant and behaves similar to “base bleed,” which refers to the injection of low-momentum fluid into the near-wake of a bluff body; this behaviour is a feature of the III_B flow pattern of Gu and Sun (1999) and the base-bleed (BB) flow pattern of Sumner et al. (2000). Some of the effects of base bleed include an increase in the vortex formation length, a reduction in drag force, and a weakening of the Kármán vortex shedding process (Bearman, 1967; Wood, 1967). For two staggered cylinders, the direction and strength of the gap flow can vary with α , being either deflected towards the upstream cylinder or the downstream cylinder, or being directed along the flow centreline (Sumner et al., 2000). In the side-by-side configuration, $\alpha = 90^\circ$, the two staggered cylinders continue to behave as if a single bluff body with base bleed (Sumner et al., 1999). The mean aerodynamic force coefficient and Strouhal number data for the closely spaced staggered cylinders are shown in Fig. 4 and selected power spectra are shown in Fig. 5.

4.1. Forces on the upstream cylinder

The behaviour of the mean aerodynamic force coefficients with incidence angle, for the upstream cylinder, is generally similar for the two pitch ratios, see Fig. 4. The mean lift coefficient for the upstream cylinder experiences large

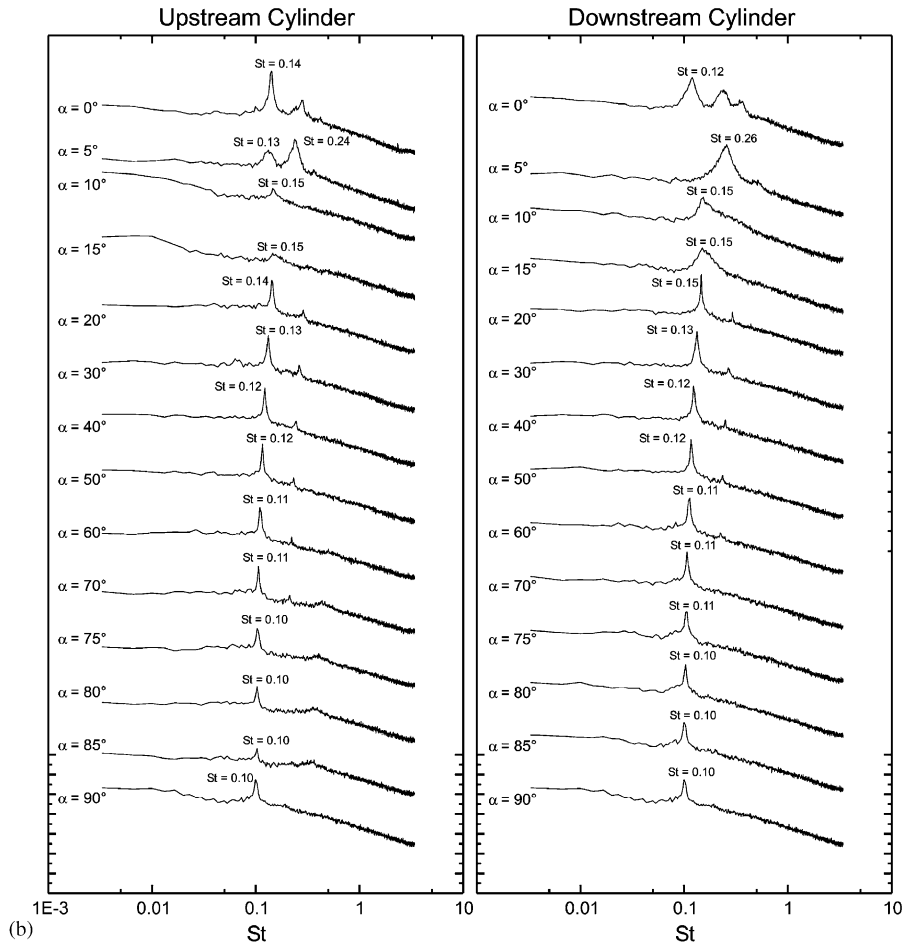


Fig. 5. (Continued)

changes in magnitude, and it may be either inward-directed (negative) or outward-directed (positive). The mean drag coefficient of the upstream cylinder may be up to 30% higher or 25% lower than the value for a single, isolated circular cylinder, depending on the incidence angle.

In the tandem configuration, $\alpha = 0^\circ$ (Fig. 4), there is zero mean lift force on the upstream cylinder. The mean drag coefficient is close to the value for a single circular cylinder. For $\alpha < 30^\circ$ (Fig. 4), the lift force on the upstream cylinder is inward-directed (negative), which means that the upstream cylinder is pulled towards the downstream cylinder. At a critical incidence angle of $\alpha \approx 9^\circ$, the lift force on the upstream cylinder attains a local maximum inward-directed value, and the drag coefficient reaches a local maximum value (as indicated in Fig. 4); this behaviour is similar for the two pitch ratios.

For $\alpha > 30^\circ$ (Fig. 4), the lift force on the upstream cylinder is outward-directed (positive), which means that the upstream cylinder is being pushed away from the downstream cylinder. The drag coefficient becomes higher than for a single circular cylinder.

For $P/D = 1.125$ (Fig. 4(a)), the maximum outward-directed lift coefficient occurs near $\alpha = 45^\circ$. This is followed by a lowering of the lift coefficient to the single-cylinder value of zero between $\alpha = 80^\circ$ and 86° , and then a sudden increase as α approaches 90° . This sudden increase is accompanied by a corresponding reduction in C_D (as indicated in Fig. 4(a)). This behaviour of the mean aerodynamic forces may be caused by changes to the base-bleed flow pattern. This behaviour is not seen for $P/D = 1.25$ (Fig. 4(b)), where the maximum outward-directed C_L occurs later at $\alpha \approx 65^\circ$. In the side-by-side configuration, $\alpha = 90^\circ$, the upstream cylinder continues to experience the repulsive lift force (Fig. 4).

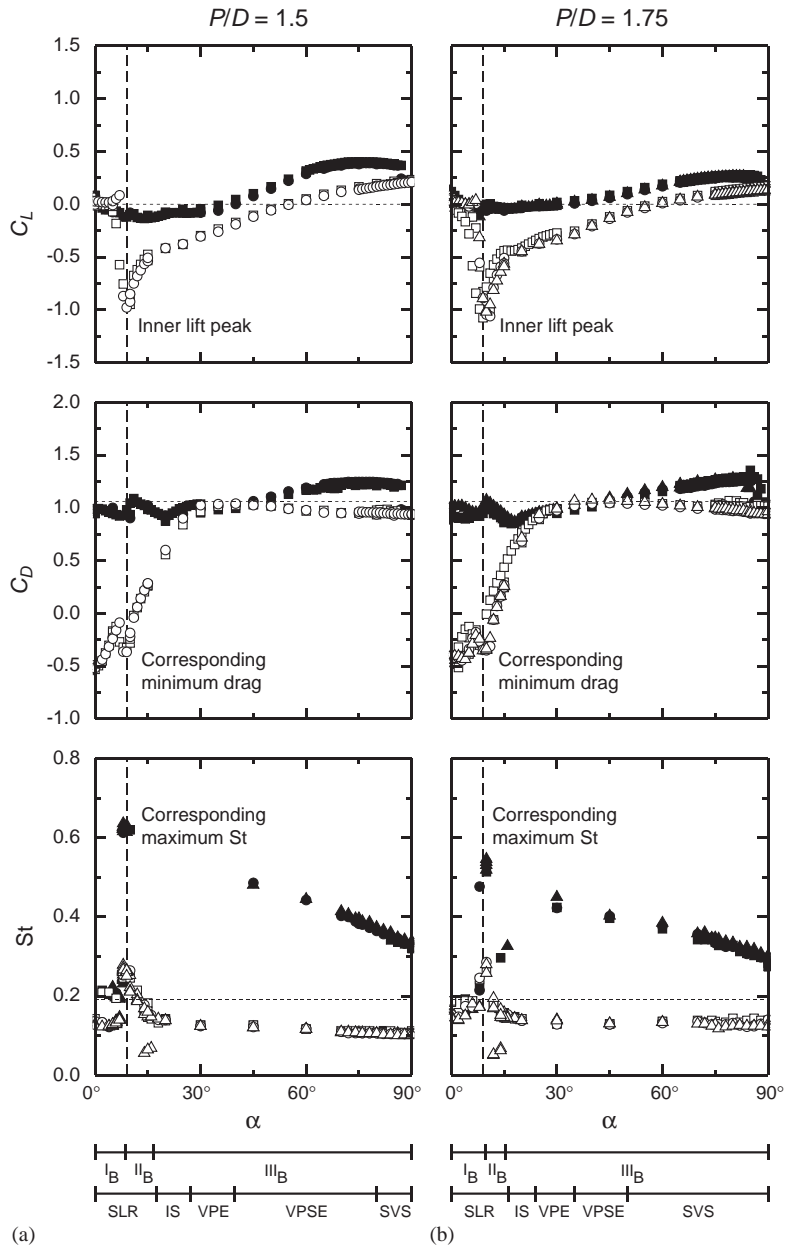


Fig. 6. Moderately spaced configurations of two staggered circular cylinders in cross-flow: (a) $P/D = 1.5$; (b) $P/D = 1.75$; (c) $P/D = 2.0$; (d) $P/D = 2.5$. Symbols as in Fig. 4. Flow pattern boundaries of Gu and Sun (1999) for $Re = 2.2 \times 10^5$: patterns I_B , II_B , and III_B . Flow pattern boundaries of Sumner et al. (2000) for $Re = 850$ – 1900 : SLR (shear layer reattachment), IS (induced separation), VPE (vortex pairing and enveloping), VPSE (vortex pairing, splitting and enveloping), and SVS (synchronized vortex shedding).

4.2. Forces on the downstream cylinder

Similar to the upstream cylinder, the behaviour of the mean aerodynamic force coefficients with incidence angle on the downstream cylinder is mostly the same for the two pitch ratios, Fig. 4. The lift coefficient for the downstream cylinder is strongly inward-directed (negative) at lower incidence angles, but becomes outward-directed (positive) at higher incidence angles. The mean drag coefficient of the downstream cylinder remains similar to, or lower than, the

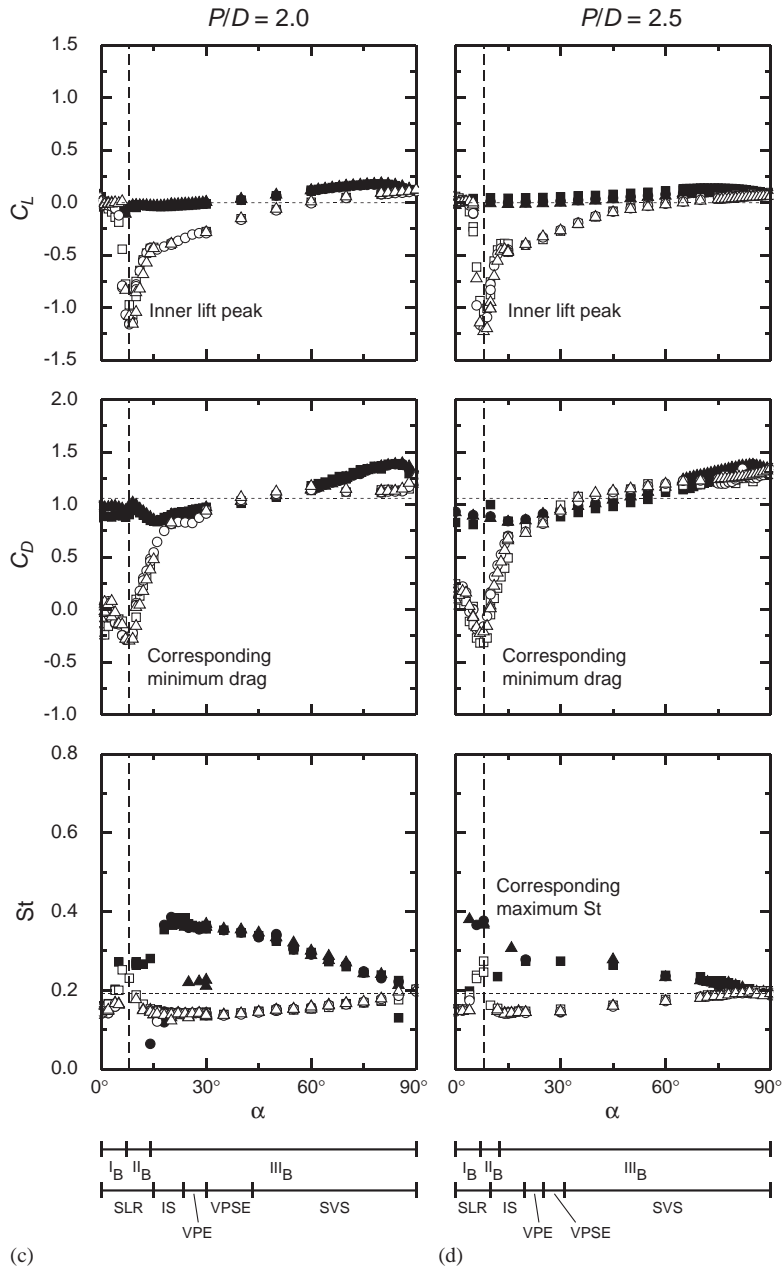


Fig. 6. (Continued)

value for a single circular cylinder. At small incidence angles, the drag force is negative, indicating that a thrust force acts upon the downstream cylinder.

In the tandem configuration, $\alpha = 0^\circ$, the mean lift force on the downstream cylinder is zero and the drag force is negative, for both P/D (Fig. 4). The downstream cylinder is completely enclosed by the shear layers from the upstream cylinder (Fig. 2(a)), and the resulting pressure distribution causes the downstream cylinder to experience a thrust force. For the closely spaced staggered cylinders, the drag coefficient of the downstream cylinder attains its most negative value ($C_D \approx -0.55$ for $P/D = 1.125$, $Re = 5.6 \times 10^4$, Fig. 4(a)) when the cylinders are in tandem.

For small non-zero incidence angles, where the cylinders are nearly tandem, the downstream cylinder continues to experience the thrust force (Fig. 4) that acts to pull the downstream cylinder into the near-wake region of the upstream

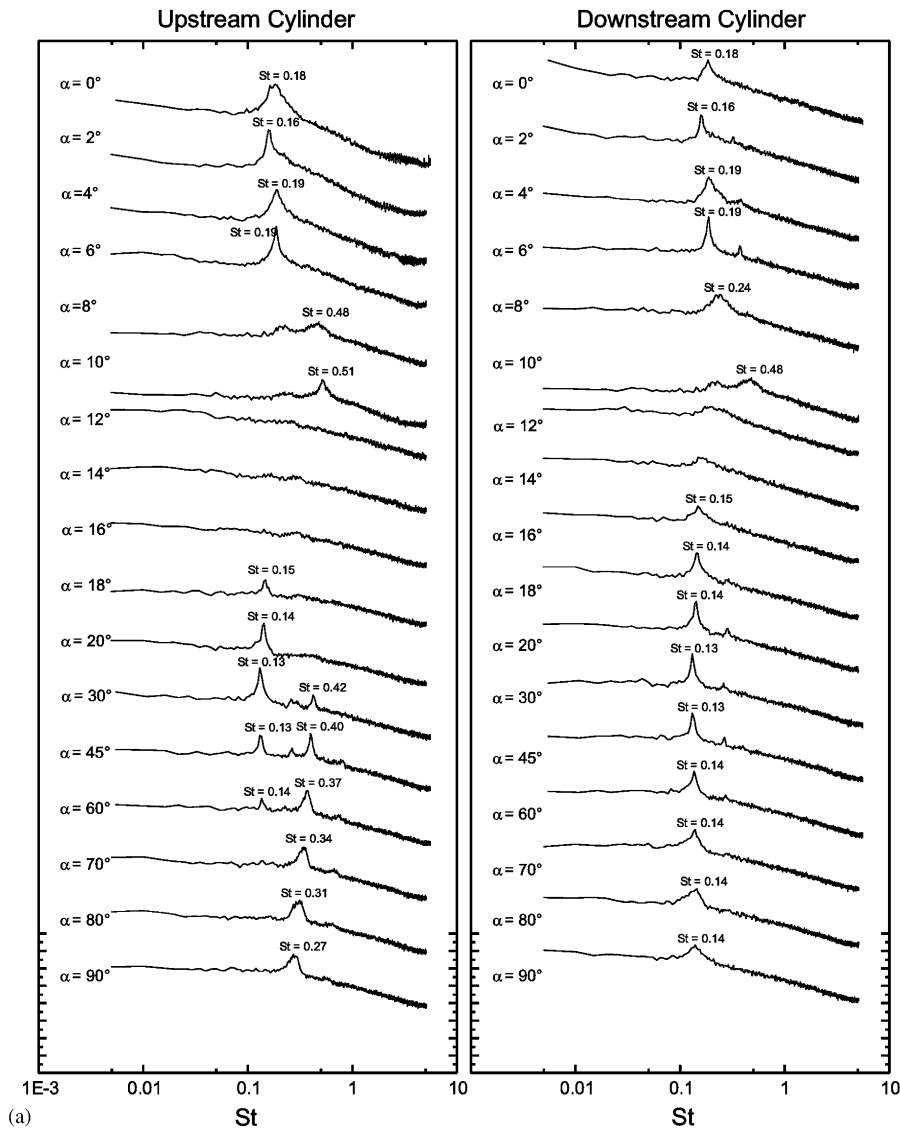


Fig. 7. Selected power spectra, as a function of incidence angle, for moderately spaced staggered cylinders: (a) $P/D = 1.75$, $Re = 3.2 \times 10^4$; (b) $P/D = 2.5$, $Re = 7.2 \times 10^4$. Each spectrum represents 250 averages. The vertical (logarithmic) scale is arbitrary, but the same scale is used for each spectrum.

cylinder. The drag coefficient increases with α , with zero drag force experienced at $\alpha \approx 13^\circ$ and 8° for $P/D = 1.125$ and 1.25 , respectively (Figs. 4(a) and (b)). Thereafter, the drag force remains positive for further increases in α .

At the same critical incidence angle identified in the data for the upstream cylinder (Section 4.1), $\alpha \approx 9^\circ$, the downstream cylinder suddenly experiences a maximum inward-directed (negative) lift force (Fig. 4). The discontinuous behaviour at $\alpha \approx 9^\circ$, and the maximum (negative) value of lift thereafter, is known as the “inner lift peak” (Zdravkovich and Pridden, 1977). The inner lift peak ($C_L \approx -0.80$ for $P/D = 1.125$, $Re = 5.6 \times 10^4$, Fig. 4(a)) coincides with a local minimum value for the drag coefficient ($C_D \approx -0.52$ for $P/D = 1.125$, $Re = 5.6 \times 10^4$, Fig. 4(a)). From the flow pattern boundaries of Gu and Sun (1999), the inner lift peak occurs at the switch from I_B to II_B .

For $\alpha > 60^\circ$, the lift force on the downstream cylinder becomes positive, or outward directed, meaning the downstream cylinder tends to be repelled away from the upstream cylinder (Fig. 4). At high α , the drag coefficient for the downstream cylinder remains close to the value for a single cylinder.

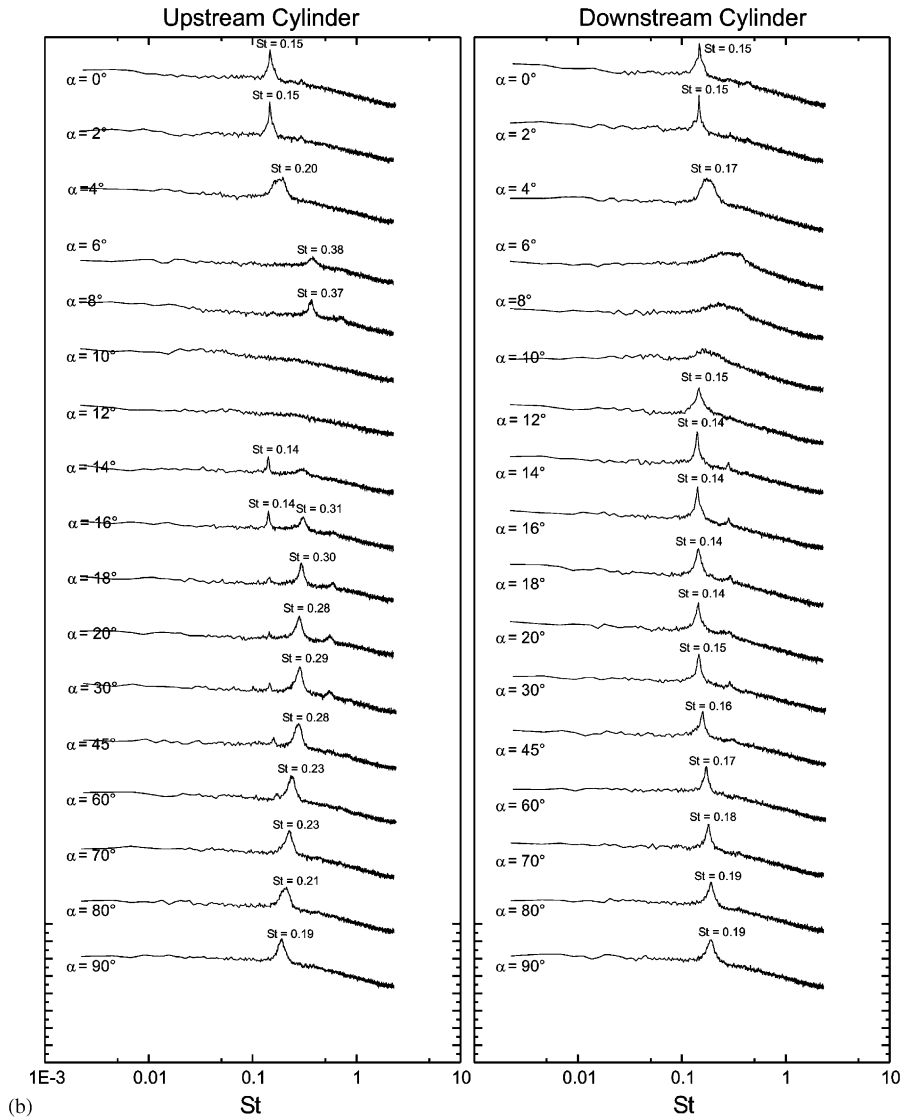


Fig. 7. (Continued)

4.3. Strouhal number data and power spectra

The general behaviour of the vortex shedding frequency data shows that the Strouhal numbers measured behind the upstream and downstream cylinders are nearly the same, which indicates that a single vortex shedding process is present (Fig. 4). The detection of a single Strouhal number is consistent with the closely spaced cylinders behaving as a single bluff body (Sumner et al., 2000), as shown by the flow patterns in Fig. 2(a). The single bluff body behaviour has also led to the definition of a universal wake number for closely spaced staggered cylinders (Sumner, 2004). When the incidence is greater than the critical incidence angle of $\alpha \approx 9^\circ$, the Strouhal number is lower than that of a single circular cylinder. The Strouhal number decreases with α to a value of $St \approx 0.1$ (one-half the vortex shedding frequency for an isolated circular cylinder). The lowering of the Strouhal number occurs as the near-wake region lengthens and widens with increasing α .

When the cylinders are nearly tandem and the incidence is less than the critical incidence angle of $\alpha \approx 9^\circ$, the Strouhal number is higher than the single-cylinder value. The peak value of St occurs at the critical incidence angle and coincides with the inner lift peak and its corresponding minimum drag (Fig. 4). The high vortex shedding frequencies measured at small incidence angles are also found in the tandem configuration (Ljungkrona et al., 1991), and are caused by a shortening and narrowing of the near-wake region compared to the case of a single cylinder (Sumner et al., 2000).

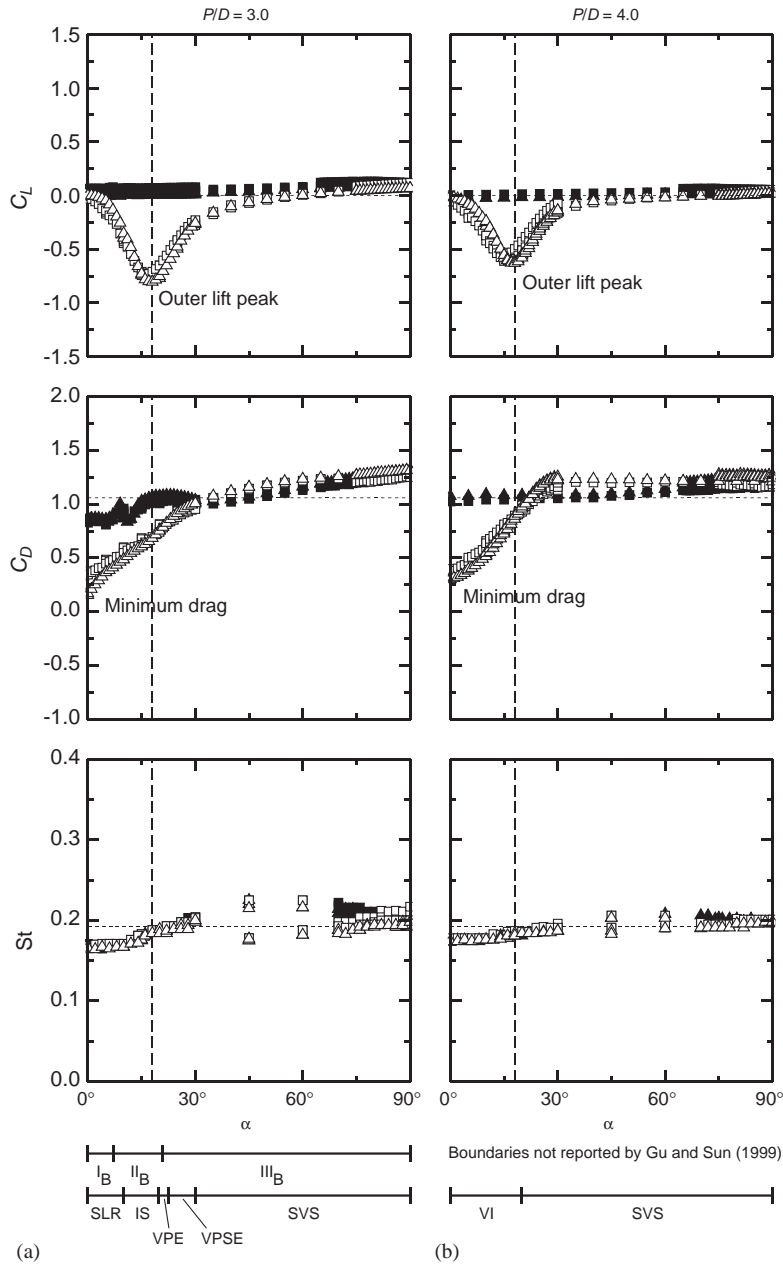


Fig. 8. Widely spaced configurations of two staggered circular cylinders in cross-flow: (a) $P/D = 3.0$; (b) $P/D = 4.0$. Symbols as in Fig. 4. Flow pattern boundaries of Gu and Sun (1999) for $Re = 2.2 \times 10^5$: patterns I_B , II_B , and III_B . Flow pattern boundaries of Sumner et al. (2000) for $Re = 850$ – 1900 : SLR (shear layer reattachment), IS (induced separation), VPE (vortex pairing and enveloping), VPSE (vortex pairing, splitting and enveloping), SVS (synchronized vortex shedding), and VI (vortex impinging).

There is also some degree of scatter in the St data when α is less than the critical incidence angle. It is seen from the power spectra in Fig. 5 that the vortex shedding peaks are smaller and more broad banded when $\alpha < 20^\circ$. For $P/D = 1.125$ (Fig. 5(a)) there was no discernible vortex shedding frequency behind the upstream cylinder at $\alpha = 5^\circ$; for $P/D = 1.25$ (Fig. 5(b)) very small vortex shedding peaks were measured behind the upstream cylinder at $\alpha = 10^\circ$ and 15° . This relationship between the behaviour of the Strouhal number and the behaviour of the aerodynamic force coefficients has also been observed for staggered configurations with higher pitch ratios (Sumner and Richards, 2003).

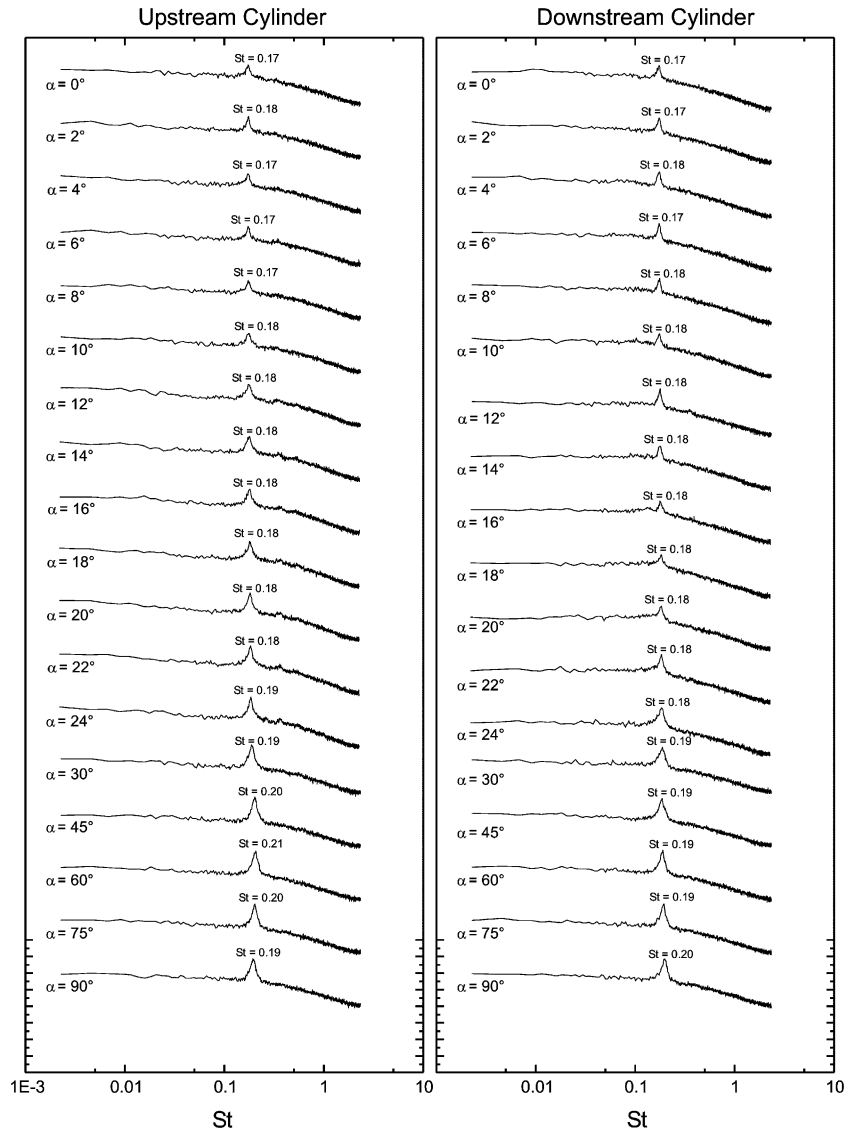


Fig. 9. Selected power spectra, as a function of incidence angle, for widely spaced staggered cylinders, $P/D = 4.0$, $Re = 7.2 \times 10^4$. Each spectrum represents 250 averages. The vertical (logarithmic) scale is arbitrary, but the same scale is used for each spectrum.

For $P/D = 1.125$ (Fig. 4(a)), there is a discontinuity in the Strouhal number between $\alpha = 60^\circ$ and 80° . As the incidence angle is increased, there is a small reduction in the Strouhal number (from $St = 0.10$ for $\alpha < 60^\circ$ to $St = 0.07$ for $\alpha > 60^\circ$) along with a change in the power spectra (Fig. 5(a)), with the peaks for the upstream and downstream cylinders becoming noticeably smaller and more broad banded for $\alpha > 60^\circ$. This behaviour of the power spectra is not seen for $P/D = 1.25$ (Fig. 5(b)). This small change in St may be related to changes in the base bleed flow pattern within the combined wake of the cylinders.

5. Moderately spaced staggered configurations

Moderately spaced staggered cylinder configurations of $P/D = 1.5, 1.75, 2.0$ and 2.5 experience a wide range of flow patterns (Fig. 2(b)) as the incidence angle and pitch ratio are varied (Sumner et al., 2000). In the tandem configuration, $\alpha = 0^\circ$, the shear layers from the upstream cylinder wrap no longer around and enclose the downstream cylinder as they

did with the closely spaced cylinders (Section 4); rather, these shear layers reattach in an alternating fashion onto the downstream cylinder and enclose a region of fluid in the gap between the cylinders (Ljungkrona and Sundén, 1993). Shear layer reattachment is maintained at small non-zero incidence angles as the inner shear layer from the upstream cylinder reattaches onto the outer side of the downstream cylinder, this being a feature of the I_B flow pattern of Gu and Sun (1999) and the SLR flow pattern of Sumner et al. (2000) described earlier. Since the cylinders are now spaced further apart than with the closely spaced staggered configurations, this reattachment is maintained only for a small range of incidence angles at the largest P/D ratios, and most flow patterns involve increasing amounts of the approach flow penetrating the gap between the cylinders and entering the near-wake region. The II_B flow pattern of Gu and Sun (1999) and the IS flow pattern of Sumner et al. (2000), which were described earlier, are observed at smaller incidence angles. As the incidence angle is increased and more of the approach flow can enter the gap between the cylinders, a distinct near-wake region forms for the first time behind the upstream cylinder, and Kármán vortex shedding occurs from both cylinders rather than from the cylinder group as a whole. The near-wake region of the upstream cylinder is short and narrow, as it is constrained by the angle of the gap flow, and thus vortex shedding from the upstream cylinder occurs at a Strouhal number much higher than the single cylinder. Vortex shedding from the wide near-wake region behind the downstream cylinder is associated with a Strouhal number lower than that of the single cylinder. The above features observed at intermediate incidence angles are common to the III_B flow pattern of Gu and Sun (1999), the vortex pairing and enveloping (VPE) flow pattern of Sumner et al. (2000), and the vortex pairing, enveloping and splitting (VPSE) flow pattern of Sumner et al. (2000). The VPE and VPSE flow patterns are so named because of the complicated vortex interactions that occur in the combined wake of the two cylinders. Vortex shedding from both cylinders is maintained at higher incidence angles up to and including the side-by-side configuration ($\alpha = 90^\circ$). The two adjacent vortex-shedding processes are synchronized to some degree, which is a feature of the synchronized vortex shedding (SVS) flow pattern of Sumner et al. (2000); Gu and Sun (1999) did not study the staggered configuration extensively at higher incidence angles. In the side-by-side configuration, two main SVS flow patterns are observed: when $P/D < 2.0$, the gap flow is biased towards one of the cylinders, one cylinder has a narrow near-wake region, and the other cylinder has a wide near-wake region; when $P/D \geq 2.0$, the gap flow is aligned in the flow direction and the near-wake regions of the two cylinders are the same size (Sumner et al., 1999, 2000). The mean aerodynamic force coefficient and Strouhal number data for the moderately spaced staggered cylinders are shown in Fig. 6 and selected power spectra are shown in Fig. 7.

5.1. Forces on the upstream cylinder

For moderately spaced staggered cylinders, the mean aerodynamic forces experienced by the upstream cylinder (Fig. 6) have much smaller variations in magnitude compared to the closely spaced staggered cylinders (Section 4.1), and a less complex behaviour than the downstream cylinder (Section 5.2). The data behave similarly for the four pitch ratios, $P/D = 1.5, 1.75, 2.0$, and 2.5 (Fig. 6). The mean lift coefficient on the upstream cylinder is small, being close to zero at lower incidence angles but attaining a small positive or outward-directed value at higher incidence angles. The general tendency of the mean lift coefficient is to become progressively smaller in magnitude as P/D is increased; for $P/D = 2.5$ (Fig. 6(d)), the lift force is nearly zero at all incidence angles. The mean drag coefficient for the upstream cylinder remains close to the single-cylinder value over nearly the entire range of α (within $\pm 30\%$ of the single-cylinder value). It attains a local maximum value that coincides with the inner lift peak (described in Section 5.2) at lower incidence angles, and is higher than the single-cylinder value at higher incidence angles.

In the tandem configuration, the flow pattern is symmetric and the lift coefficient for the upstream cylinder is zero. An enclosed recirculation zone exists between the two cylinders, which causes the mean drag coefficient of the upstream cylinder to be smaller than the single-cylinder value (Ljungkrona and Sundén, 1993; Sumner et al., 2000).

For small incidence angles, $\alpha < 30^\circ$, the lift coefficient of the upstream cylinder attains either a very small negative value (inward-directed) or is zero (Fig. 6), and the drag coefficient of the upstream cylinder remains slightly lower than the single-cylinder value (Fig. 6). The drag coefficient attains a local maximum value between $\alpha \approx 7^\circ$ and 11° (Fig. 6), which is found to coincide with the inner lift peak for the downstream cylinder (Section 5.2). In this range of α the flow pattern involves some form of shear layer reattachment or very weak gap flow (Fig. 2(b)), which are features of the I_B and II_B flow patterns of Gu and Sun (1999).

At larger incidence angles, the mean lift coefficient on the upstream cylinder is positive (outward directed), indicating the cylinders tend to repel one another. When $\alpha > 45^\circ$ the mean drag coefficient becomes greater than the single-cylinder value.

For $P/D = 1.5$ and 1.75 only (Figs. 6(a) and (b)), there is a small discontinuity in the mean lift and drag coefficients at $\alpha = 86^\circ$. This discontinuity may indicate a switch to a biased flow pattern, which is a characteristic at similar P/D ratios of the side-by-side configuration, $\alpha = 90^\circ$ (Sumner et al., 1999), and staggered configurations that are nearly

side-by-side (Price and Paidoussis, 1984; Zdravkovich, 1987; Gu and Sun, 1999; Sumner et al., 2000). This discontinuity is not apparent at $P/D = 2.0$ and 2.5 (Figs. 6(c), (d)) where the biased flow pattern is not observed in the side-by-side configuration (Sumner et al., 1999).

5.2. Forces on the downstream cylinder

For the moderately spaced staggered configurations, the behaviour of the mean aerodynamic forces is similar for the four pitch ratios, $P/D = 1.5, 1.75, 2.0,$ and 2.5 (Fig. 6). The behaviour of the force coefficients on the downstream cylinder is similar to what was found for the closely staggered configurations (Section 4.2), including the inner lift peak and its corresponding minimum drag force (Fig. 6).

In the tandem configuration, $\alpha = 0^\circ$, the downstream cylinder experiences zero mean lift coefficient because the flow pattern is symmetric. The mean drag coefficient of the downstream cylinder at $\alpha = 0^\circ$ is lower than the single-cylinder value for all four pitch ratios. Its value increases with the pitch ratio, from negative values (indicating the downstream cylinder experiences a thrust force) of $C_D = -0.52$ and -0.48 at $P/D = 1.5$ and 1.75 (Figs. 6(a) and (b)), respectively, to a small positive value of $C_D = 0.16$ at $P/D = 2.5$ (Fig. 6(d)). For the moderately staggered configurations of $P/D = 1.5$ and 1.75 only, the minimum mean drag coefficient values for the downstream cylinder occur at $\alpha = 0^\circ$ [contrary to what was reported by Zdravkovich and Pridden (1977)]. For the staggered configurations of $P/D = 2.0$ and 2.5 , the minimum drag for the downstream cylinder occurs at the non-zero critical incidence angle corresponding to the inner lift peak, as discussed below.

The inner lift peak is found at lower incidence angles, $\alpha < 30^\circ$, and occurs at a critical incidence angle of between $\alpha \approx 7^\circ$ and 11° (Fig. 6); this location is similar to the value of $\alpha \approx 9^\circ$ for the closely spaced staggered configurations (Section 4.2). The inner lift peak, which corresponds to the maximum value (that is, the most negative value) of the inward-directed mean lift coefficient on the downstream cylinder, becomes increasingly negative, or more strongly inward directed, as the pitch ratio is increased; its value changes from $C_L = -0.98$ at $P/D = 1.5$ (Fig. 6(a)) to $C_L = -1.20$ at $P/D = 2.5$ (Fig. 6(d)). As α is increased from the critical incidence angle (as the cylinders become more side-by-side), there is a loss of inward-directed lift; this loss of lift becomes more abrupt at higher pitch ratios (Fig. 6). As α is decreased from the critical incidence angle (as the cylinders become more tandem), there is also a sudden loss of lift: for $P/D = 1.5$ and 1.75 (Figs. 6(a) and (b)), the lift force changes from inward-directed to outward-directed; for $P/D = 2.0$ and 2.5 (Figs. 6(c), (d)), the lift force disappears.

A second local minimum drag coefficient coincides with the inner lift peak, $\alpha \approx 7^\circ$ to 11° (Fig. 6). Its value is negative for all four pitch ratios indicating that the downstream cylinder experiences a thrust force, which draws this cylinder into the near-wake region of the upstream cylinder. As the pitch ratio is increased from $P/D = 1.5$ (Fig. 6(b)) to $P/D = 2.5$ (Fig. 6(d)), this minimum drag coefficient at the critical incidence angle becomes smaller in magnitude, increasing from $C_D = -0.37$ at $P/D = 1.5$ (Fig. 6(a)) to $C_D = 0.19$ at $P/D = 2.5$ (Fig. 6(d)).

At higher incidence angles, the mean lift coefficient on the downstream cylinder slowly transitions from inward-directed (negative) to outward-directed (positive). In the side-by-side configuration, $\alpha = 90^\circ$, there remains a positive lift force on the downstream cylinder for $P/D = 1.5, 1.75$ and 2.0 (Figs. 6(a)–(c)), indicating the two cylinders experience a repulsive force. This outward-directed (repulsive) lift force is not observed for $P/D = 2.5$ (Fig. 6(d)), the lift force being zero when in the side-by-side configuration, $\alpha = 90^\circ$. This disappearance of the lift force on the downstream cylinder, at $P/D = 2.5$, is consistent with the flow pattern changes observed for the side-by-side configuration, where $P/D \approx 2.2$ marks the end of the biased flow regime (Sumner et al., 1999).

5.3. Strouhal number data and power spectra

At moderate pitch ratios, the behaviour of the Strouhal number data (Fig. 6) is more complex than that of the closely spaced cylinders (Fig. 4). For a wide range of incidence angles, two distinct Strouhal numbers are measured (Fig. 6) and there is considerable variation in the corresponding power spectra (Fig. 7). Based on the measurement location, the higher Strouhal number broadly corresponds to the upstream cylinder and the other, lower Strouhal number broadly corresponds to the downstream cylinder, as shown in the power spectra (Fig. 7).

At lower incidence angles, $\alpha < 30^\circ$, there is some scatter in the Strouhal number data, particularly for the downstream cylinder (Fig. 6). For $P/D = 1.5$ and 1.75 , this scatter can be attributed to a weakened vortex shedding process when the cylinders are nearly tandem, as seen by the broad banded and irregularly shaped peaks in the power spectra (Fig. 7(a)). For $P/D = 2.0$ and 2.5 , however, these peaks are more sharply defined (Fig. 7(b)). A very high Strouhal number is found at the critical incidence angle, $\alpha \approx 7$ – 11° , corresponding to the inner lift peak and its associated minimum drag coefficient (Section 5.2). The peak in the power spectrum for this very high frequency is sharper and better defined when it is measured behind the upstream cylinder (Fig. 7), but was also found behind the downstream cylinder for $P/D = 1.75$

(Fig. 7(a)). The magnitude of this Strouhal number decreases with P/D , attaining a value of $St \approx 0.6$ at $P/D = 1.5$ (Fig. 6(a)) and a value of $St \approx 0.4$ at $P/D = 2.5$ (Fig. 6(d)).

At incidence angles slightly larger than the critical incidence angle, the peaks in the power spectra are either broad-banded or absent, indicating a weakening or suppression of vortex shedding from the cylinders (Fig. 7). This phenomenon was previously reported by Sumner and Richards (2003) for $P/D = 2.0$ and 2.5 , but from the present study it has now been shown to exist throughout the range of moderately spaced staggered configurations, $1.5 \leq P/D \leq 2.5$. For $P/D = 1.75$, the peaks are absent from the power spectra at $\alpha = 12\text{--}16^\circ$ for the upstream cylinder and at $\alpha = 12^\circ$ and 14° for the downstream cylinder (Fig. 7(a)); for $P/D = 2.5$, the peaks are absent from the power spectra at $\alpha = 10^\circ$ and 12° for the upstream cylinder and at $\alpha = 10^\circ$ for the downstream cylinder (Fig. 7(b)). For $P/D = 2.5$, vortex shedding resumes at a lower incidence angle, because the gap between the cylinders is wider. Similar behaviour (although vortex shedding activity was never completely suppressed) was found for the closely spaced staggered cylinders (Section 4.3). This suppression of vortex shedding coincides with the Π_B flow pattern of Gu and Sun (1999).

The reappearance of the vortex shedding peaks in the power spectra, at $\alpha = 16\text{--}18^\circ$ for $P/D = 1.75$ (Fig. 7(a)) and at $\alpha = 12\text{--}14^\circ$ for $P/D = 2.5$ (Fig. 7(b)), coincides with the transition to the III_B flow pattern of Gu and Sun (1999), which involves vortex shedding from both the upstream and downstream cylinders (Fig. 2(b)). The reappearance of vortex shedding first occurs as a single low frequency that is measured behind both cylinders, corresponding to $St = 0.13\text{--}0.15$ (Figs. 6 and 7). For the downstream cylinder, this low frequency persists as α is increased to 90° , and is associated with alternate vortex shedding from this cylinder (Sumner et al., 2000). For $P/D = 1.75$ (Fig. 7(a)), a second, higher frequency appears in the power spectrum for the upstream cylinder when $\alpha \geq 30^\circ$. This high frequency persists as α is increased to 90° , and is associated with vortex shedding from the upstream cylinder. For $\alpha = 30\text{--}60^\circ$, both the high and low frequencies are detected in the power spectra for the upstream cylinder (Fig. 7(a)). Similar behaviour is seen in the power spectra for $P/D = 2.5$ (Fig. 7(b)), although the appearance of the two vortex shedding peaks behind the upstream cylinder is seen only at $\alpha = 16^\circ$ because of the reduced interference between the cylinders.

For $P/D = 1.75$, the vortex shedding peaks in the power spectra (Fig. 7(a)) become more broad-banded for $\alpha > 60^\circ$, particularly for the downstream cylinder. This may indicate a change in the near-wake flow pattern at these high incidence angles, as suggested earlier (Section 5.1) by the discontinuity in the upstream cylinder force coefficient data for $P/D = 1.5$ and 1.75 (Figs. 6(a) and (b)) at $\alpha = 86^\circ$. As the incidence angle is increased to $\alpha = 90^\circ$, and as the pitch ratio is increased from $P/D = 1.5$ to 2.5 , the difference between these two Strouhal numbers becomes progressively smaller, and their values become closer to that of a single circular cylinder (Fig. 6). For $P/D = 1.5$ and 1.75 (Figs. 6(a) and (b)), two different Strouhal numbers are measured when the cylinders are side-by-side, $\alpha = 90^\circ$. This is the result of the biased flow pattern, which is characteristic of the side-by-side configuration at these pitch ratios. In the biased flow pattern, the flow through the gap between the two cylinders is deflected towards one of the cylinders, and each cylinder has a different size of near-wake region and a different vortex shedding frequency (Sumner et al., 1999). The biased flow pattern is not found at $P/D = 2.0$ and 2.5 (Figs. 6(c) and (d)), and therefore a single Strouhal number is measured when the cylinders are side-by-side.

6. Widely spaced staggered configurations

Widely spaced staggered configurations, which correspond to $P/D = 3.0$ and 4.0 , were primarily distinguished by changes to the behaviour of the mean lift coefficient of the downstream cylinder and the Strouhal number data in general. The force coefficient and Strouhal number data for the widely spaced staggered configurations are given in Fig. 8. Power spectra are given in Fig. 9. Flow patterns representative of widely spaced staggered configurations were shown in Fig. 2(c).

In the tandem configuration, $\alpha = 0^\circ$, the shear layers from the upstream cylinder alternately reattach onto the downstream cylinder at $P/D = 3.0$, see Fig. 2(c). However, at $P/D = 4.0$, the downstream cylinder is located too far from the upstream cylinder for shear layer reattachment to occur, and there will be Kármán vortex shedding from the upstream cylinder. Vortex shedding then occurs from both cylinders. The loss of shear layer reattachment occurs at a critical pitch ratio between $P/D = 3.0$ and 4.0 . Studies of two cylinders in tandem have shown that the critical pitch ratio is sensitive to the Reynolds number and other experimental conditions, but falls within $3.0 < P/D < 4.0$ in the subcritical regime (Ljungkrona and Sundén, 1993).

For staggered configurations, shear layer reattachment will generally not occur because of the large spacing between the cylinders, and there will be Kármán vortex shedding from both cylinders for both $P/D = 3.0$ and 4.0 , see Fig. 2(c). At smaller incidence angles, $\alpha = 15^\circ$, the Kármán vortices shed from the upstream cylinder impinge upon, and interact with, the downstream cylinder and its vortex shedding process (Sumner et al., 2000). At higher incidence angles, $\alpha = 60^\circ$, two vortex shedding processes will occur adjacent to one another. This same flow pattern is

observed in the side-by-side configuration, $\alpha = 90^\circ$, where the vortex streets may become synchronized (Sumner et al., 1999, 2000).

6.1. Forces on the upstream cylinder

For widely spaced staggered cylinders, the mean aerodynamic forces on the upstream cylinder (Fig. 8) are mostly similar to those experienced by a single, isolated circular cylinder. The mean drag coefficient remains close to the single-cylinder value for most incidence angles. There is nearly zero mean lift force at all incidence angles, except in the nearly side-by-side configuration, $\alpha = 90^\circ$, where the mean lift coefficient attains a small positive value (outward directed).

At small α , for $P/D = 3.0$ (Fig. 8(a)), the drag force acting upon the upstream cylinder becomes smaller than the single-cylinder value, and exhibits local maximum and minimum values. This behaviour is unchanged from what was observed for moderately spaced staggered configurations (see $P/D = 2.5$, Fig. 6(d), for example). However, for $P/D = 4.0$ (Fig. 8(b)), the drag force remains constant, at the single-cylinder value. This change in behaviour for $P/D = 4.0$ indicates that there is now Kármán vortex shedding from the upstream cylinder, including at $\alpha = 0^\circ$.

At high α , up to and including the side-by-side configuration, at $\alpha = 90^\circ$, the drag coefficient becomes higher than the single-cylinder value (Fig. 8). Also, the mean lift coefficient attains a small, positive value for both P/D ratios, indicating the upstream cylinder experiences a small repulsive force. The lift force decreases in magnitude with an increase in pitch ratio; for example, at $Re = 3.2 \times 10^4$, the magnitude of the lift coefficient decreases from $C_L = 0.09$ to 0.04 when the pitch ratio is changed from $P/D = 3.0$ to 4.0. This behaviour is consistent with the flow around side-by-side cylinders, which shows proximity interference effects up to $P/D = 5.0$ (Sumner et al., 1999).

6.2. Forces on the downstream cylinder

For the downstream cylinder, the location of the maximum inward-directed lift force (Fig. 8) shifts to a higher incidence angle compared to the closely and moderately spaced staggered cylinder configurations (Figs. 4 and 6). This shift in the critical incidence angle, from $\alpha \approx 9^\circ$ for moderately spaced staggered arrangements ($P/D = 1.5$ – 2.5 , Fig. 6) to $\alpha \approx 18^\circ$ for widely spaced arrangements ($P/D = 3.0$ and 4.0, Fig. 8), denotes the appearance of the “outer lift peak” (Zdravkovich and Pridden, 1977; Ting et al., 1998). The outer lift peak becomes less negative with an increase in the pitch ratio, which reflects the reduced interference of the two cylinders as the spacing is increased. The outer lift peak may be attributed to the vortex impingement process and the proximity of the vortex street wake from the upstream cylinder, and therefore does not appear or disappear suddenly with a change in incidence angle.

In contrast to the inner lift peak, the outer lift peak does not coincide with a minimum drag force (Fig. 8). Rather, there is now only one drag force minimum (as opposed to two minimum values, for the closely and moderately spaced cylinders), which occurs when the widely spaced cylinders are in tandem, $\alpha = 0^\circ$. The drag coefficient is positive at all incidence angles, i.e. the downstream cylinder at no time experiences a thrust force; this is another distinguishing feature of widely spaced staggered cylinders. The drag coefficient of the downstream cylinder increases and approaches the single-cylinder value as α is increased and the interference between the two cylinders is reduced (Fig. 8). In the nearly side-by-side configuration the drag coefficient of the downstream cylinder remains higher than the single cylinder value for both $P/D = 3.0$ and 4.0 (Fig. 8), similar to the upstream cylinder. For the widely spaced configurations of $P/D = 3.0$ and 4.0, the inner lift peak is not detected.

6.3. Strouhal number data and power spectra

At large pitch ratios, the same Strouhal number is measured behind both cylinders for most incidence angles, see Fig. 8. Both cylinders, therefore, undergo vortex shedding at the same frequency; Fig. 2(c). This Strouhal number remains close to that of a single circular cylinder indicating the reduced effects of interference between the cylinders. Two distinct Strouhal numbers are measured, however, at intermediate and high incidence angles, but the difference between them is small, particularly for $P/D = 4.0$, Fig. 8(b). This less complex behaviour of the Strouhal number contrasts with the behaviour of the aerodynamic forces on the downstream cylinder, particularly at smaller incidence angles, Fig. 8, where the outer lift peak and minimum drag force occur. Evidence of the outer lift peak is seen only in the power spectra for the downstream cylinder (Fig. 9), where the vortex shedding peak is reduced in strength at incidence angles about the outer lift peak, $\alpha = 18^\circ$. The broadening and weakening of the vortex shedding peak at lower incidence angles (Fig. 9) may be attributed to the impingement onto the downstream cylinder (or proximity to this cylinder) of Kármán vortices shed from the upstream cylinder [the VI flow pattern of Sumner et al. (2000)], and the interaction of its Kármán vortex street with the flow field of the downstream cylinder.

7. Conclusions

An experimental investigation was undertaken of the mean aerodynamic forces and Strouhal numbers for a pair of circular cylinders in the subcritical Reynolds number regime, $Re = 3.2 \times 10^4$ – 7.4×10^4 . The two circular cylinders, of equal diameter, were arranged in the staggered configuration. The mean aerodynamic force coefficients and Strouhal numbers were obtained for both the upstream and downstream cylinders, for very small increments in the incidence angle, α , and for pitch ratios from $P/D = 1.125$ to 4.0. The behaviour of the aerodynamic force coefficients and Strouhal numbers was related to the changes in the reported flow patterns, and could be broadly classified by the pitch ratio according to whether the staggered cylinders were closely spaced, moderately spaced, or widely spaced. Previous studies in the literature have not reported extensive measurements of the forces on the upstream cylinder. The use of very small increments in α in the present study has revealed new information on the behaviour of the forces and Strouhal number data for both cylinders.

For closely spaced staggered configurations, $P/D = 1.125$ and 1.25, the mean aerodynamic forces on both the upstream and downstream cylinders vary significantly with the incidence angle. Although the flow pattern for closely spaced cylinders is similar to a single bluff body, shear layer reattachment at small incidence angles, and base-bleed gap flow at large incidence angles, have profound effects on the forces experienced by each cylinder. In addition to the inner lift peak for the downstream cylinder, several other critical incidence angles were identified, for both cylinders, which corresponded to local minimum or maximum values of the lift or drag forces, or a discontinuity.

For moderately spaced staggered configurations, $P/D = 1.5$ – 2.5 , the flow pattern undergoes a number of changes with the incidence angle. Notable features are the inner lift peak, a corresponding minimum drag and high value of the Strouhal number, and a loss of lift with increasing α that becomes increasingly abrupt with P/D . The power spectra of the velocity fluctuations at incidence angles near the inner lift peak are characterized by broad-banded peaks or an absence of sharply defined peaks. The sudden appearance or disappearance of periodic vortex shedding activity at small incidence angles, which may occur if the mean flow direction varies, is problematic for the reliable prediction of vortex-induced vibrations in staggered cylinder configurations. At higher α , when there is vortex shedding from the two cylinders, both experience outward-directed lift forces.

For widely spaced staggered configurations, $P/D = 3.0$ and 4.0, the two cylinders behave more independently, as single, isolated circular cylinders. Both cylinders undergo Kármán vortex shedding for the entire range of α , although vortex impingement on the downstream cylinder occurs at small α . The forces on the upstream cylinder are mostly unchanged from a single cylinder, except in the tandem and side-by-side configurations, where some interference from the downstream cylinder remains. For the downstream cylinder at small α , the outer lift peak replaces the inner lift peak and there is no corresponding minimum drag.

Acknowledgments

The authors are grateful for the financial support of the Natural Sciences and Engineering Research Council of Canada (NSERC), the University of Saskatchewan President's NSERC Fund, and the Department of Mechanical Engineering. The assistance of D. Deutscher and Engineering Shops was greatly appreciated.

References

- Akosile, O.O., Sumner, D., 2003. Staggered circular cylinders immersed in a uniform planar shear flow. *Journal of Fluids and Structures* 18, 613–633.
- Bearman, P.W., 1967. The effect of base bleed on the flow behind a two-dimensional model with a blunt trailing edge. *The Aeronautical Quarterly* 18, 207–224.
- Bokaian, A., Geoola, F., 1984. Wake displacement as cause of lift force on cylinder pair. *Journal of Engineering Mechanics* 111, 92–99.
- Chen, S.S., 1987. *Flow-Induced Vibration of Circular Cylindrical Structures*. Hemisphere Publishing Corporation, Washington, DC.
- Cooper, K.R., 1974. Wind tunnel measurements of the steady aerodynamics forces on a smooth circular cylinder immersed in the wake of an identical cylinder. National Research Council of Canada, LTR-LA-119.
- Gu, Z.F., Sun, T.F., 1999. On interference between two circular cylinders in staggered arrangement at high subcritical Reynolds numbers. *Journal of Wind Engineering and Industrial Aerodynamics* 80, 287–309.
- Gu, Z.F., Sun, T.F., He, D.X., Zhang, L.L., 1993. Two circular cylinders in high-turbulence flow at supercritical Reynolds number. *Journal of Wind Engineering and Industrial Aerodynamics* 49, 379–388.
- Ishigai, S., Nishikawa, E., Nishimura, K., Cho, K., 1972. Experimental study of structure of gas flow in tube banks with tube axes normal to flow (Part I, Kármán vortex flow from two tubes at various spacings). *Bulletin of the JSME* 15, 949–956.

- Ishigai, S., Nishikawa, E., Yagi, E., 1973. Structure of gas flow and vibration in tube banks with tube axes normal to flow. Proceedings, International Symposium on Marine Engineering, Tokyo, Japan, pp. 1-5-2 to 1-15-33.
- Jester, W., Kallinderis, Y., 2003. Numerical study of incompressible flow about fixed cylinder pairs. *Journal of Fluids and Structures* 17, 561–577.
- Kiya, M., Arie, M., Tamura, H., Mori, H., 1980. Vortex shedding from two circular cylinders in staggered arrangement. *ASME Journal of Fluids Engineering* 102, 166–173.
- Ljungkrona, L., Sundén, B., 1993. Flow visualization and surface pressure measurement on two tubes in an inline arrangement. *Experimental Thermal and Fluid Science* 6, 15–27.
- Ljunkrona, L., Norberg, C., Sundén, B., 1991. Free-stream turbulence and tube spacing effects on surface pressure fluctuations for two tubes in an in-line arrangement. *Journal of Fluids and Structures* 5, 701–727.
- Mittal, S., Kumar, V., Raghuvanshi, A., 1997. Unsteady incompressible flows past two cylinders in tandem and staggered arrangements. *International Journal for Numerical Methods in Fluids* 25, 1315–1344.
- Moriya, M., Sakamoto, H., 1985. Fluctuating fluid forces acting on a downstream circular cylinder in the staggered arrangement. *Transactions of the JSME* 51, 2098–2104 (in Japanese).
- Nishimura, T., 1986. Flow across tube banks. In: Chermisinoff, N.P. (Ed.), *Encyclopedia of Fluid Mechanics—Flow Phenomena and Measurement*, vol. 1. Gulf Publishing Company, Houston, pp. 763–785.
- Ohya, Y.O., Okajima, A., Hayashi, M., 1989. Wake interference and vortex shedding. In: Chermisinoff, N.P. (Ed.), *Encyclopedia of Fluid Mechanics—Aerodynamics and Compressible Flow*, vol. 8. Gulf Publishing Company, Houston, pp. 322–389.
- Ozono, S., Oda, J., Yoshida, Y., Wakasugi, Y., 2001. Critical nature of the base pressure of the upstream circular cylinder in two staggered ones in cross-flow. *Theoretical and Applied Mechanics*, vol. 50, Proceedings of the 50th Japan National Congress on Theoretical and Applied Mechanics, January 23–25, 2001, Tokyo, pp. 335–340.
- Price, S.J., 1976. The origin and nature of the lift force on the leeward of two bluff bodies. *The Aeronautical Quarterly* 27, 154–168.
- Price, S.J., Païdoussis, M.P., 1984. The aerodynamic forces acting on groups of two and three circular cylinders when subject to a cross-flow. *Journal of Wind Engineering and Industrial Aerodynamics* 17, 329–347.
- Sumner, D., 2004. Closely spaced circular cylinders in cross-flow and a universal wake number. *ASME Journal of Fluids Engineering* 126, 245–249.
- Sumner, D., Richards, M.D., 2003. Some vortex-shedding characteristics of the staggered configuration of circular cylinders. *Journal of Fluids and Structures* 17, 345–350.
- Sumner, D., Wong, S.S.T., Price, S.J., Païdoussis, M.P., 1999. Fluid behaviour of side-by-side circular cylinders in steady cross-flow. *Journal of Fluids and Structures* 13, 309–338.
- Sumner, D., Price, S.J., Païdoussis, M.P., 2000. Flow-pattern identification for two staggered circular cylinders in cross-flow. *Journal of Fluid Mechanics* 411, 263–303.
- Sun, T.F., Gu, Z.F., He, D.X., Zhang, L.L., 1992. Fluctuating pressure on two circular cylinders at high Reynolds numbers. *Journal of Wind Engineering and Industrial Aerodynamics* 41–44, 577–588.
- Suzuki, N., Sato, H., Iuchi, M., Yamamoto, S., 1971. Aerodynamic forces acting on circular cylinders arranged in a longitudinal row. *Wind Effects on Buildings and Structures, International Wind Conference, Tokyo, Part II*, pp. 20–1 to 20–10.
- Szepessy, S., 1993. On the control of circular cylinder flow by end plates. *European Journal of Mechanics B/Fluids* 12, 217–244.
- Ting, D.S.-K., Wang, D.J., Price, S.J., Païdoussis, M.P., 1998. An experimental study on the fluidelastic forces for two staggered circular cylinders in cross-flow. *Journal of Fluids and Structures* 12, 259–294.
- Wardlaw, R.L., Cooper, K.R., 1973. A wind tunnel investigation of the steady aerodynamic forces on smooth and stranded twin bundled power conductors for the Aluminum Company of America. National Research Council of Canada, LTR-LA-117.
- Wood, C.J., 1967. Visualization of an incompressible wake with base bleed. *Journal of Fluid Mechanics* 29 (2), 259–272.
- Zdravkovich, M.M., 1977. Review of flow interference between two circular cylinders in various arrangements. *ASME Journal of Fluids Engineering* 99, 618–633.
- Zdravkovich, M.M., 1987. The effects of interference between circular cylinders in cross flow. *Journal of Fluids and Structures* 1, 239–261.
- Zdravkovich, M.M., 1993. Interstitial flow field and fluid forces. In: Au-Yang, M.K. (Ed.), *Technology for the 90s: A Decade of Progress*. ASME, New York.
- Zdravkovich, M.M., 2003. *Flow Around Circular Cylinders*, vol. 2. Oxford University Press, Oxford, UK.
- Zdravkovich, M.M., Pridden, D.L., 1977. Interference between two circular cylinders; series of unexpected discontinuities. *Journal of Industrial Aerodynamics* 2, 255–270.